Single component white-OLEDs derived from tris(β-diketonato) europium(III) complexes bearing the large bite angle N^N 2-(4-Thiazolyl)benzimidazole ligand

Rashid Ilmi,*[a] Jiaxuan Yin,[b] José D. L. Dutra,[c] Nawal K. Al Rasbi,[a] Willyan F. Oliveira[c], Liang Zhou,*[b] Wai-Yeung Wong,*[d] Paul R. Raithby*[e], and Muhammad S. Khan*[a]

[a]Department of Chemistry, Sultan Qaboos University, P. O. Box 36, Al Khod 123, Oman

[b]State Key Laboratory of Rare Earth Resource Utilization, Changchun Institute of Applied Chemistry, Chinese Academy of Sciences, Renmin Street 5625, Changchun 130022, People's Republic of China.
[c]Pople Computational Chemistry Laboratory, Department of Chemistry, UFS, 49100-000 São Cristóvão, Sergipe, Brazil.
[d]Department of Applied Biology and Chemical Technology, The Hong Kong Polytechnic University, Hung Hom, Kowloon, Hong Kong, People's Republic of China.
[e]Department of Chemistry, University of Bath, Claverton Down, Bath, BA2 7AY, UK
[e]Department of Chemistry, University of Bath, Claverton Down, Bath BA2 7AY, UK.

E-mail addresses and ORCID ID of corresponding authors:

Rashid Ilmi (RI)　　　: rashidilmi@gmail.com; 0000-0002-5165-5977

Liang Zhou (LZ)　　　: zhoul@ciac.ac.cn; 0000-0002-2751-5974

Wai-Yeung Wong (WYW) : wai-yeung.wong@polyu.edu.hk; 0000-0002-9949-752

Paul R. Raithby　　　: p.r.raithby@bath.ac.uk; 0000-0002-2944-0662

Muhammad S. Khan (MSK)　: msk@squ.edu.om; 0000-0001-5606-6832

Electronic Supporting Information

1. Theoretical Details

1.1 Determination of Ground State Geometry and Singlet and Triplet State Energy Levels of the Complexes

The geometry of the **Eu1** and **Eu2** complexes was optimized with the PBE1PBE and B3LYP hybrid functionals, implemented into ORCA 5.0.3 [1], and the SVP (polarized split-valence), TZVP (polarized valence triple-zeta) basis sets were used with both the B3LYP and PBE1PBE functionals. It was revealed in previous works involving other lanthanide complexes coordinated to β-diketonate ligands, conducted by our research group [2], that such functional/basis set combinations had a good cost-benefit. The crystallographic geometry of **Eu1** and **Eu2** were considered as input for the geometry optimization of the complexes. While SVP basis set considers the (4s1p)/[2s1p] electronic structure for the hydrogen atom, (7s4p1d)/[3s2p1d] for the atoms of the second period of the p-block and (10s7p1d)/[4s3p1d] for the S atom, TZVP basis set treats the corresponding electronic structure by (5s1p)/[3s1p], (11s6p1d)/[5s3p1d] and (14s9p1d)/[5s4p1d], respectively. To evaluate a basis set containing a larger number of components, the geometry optimization using the def2-TZVPPD basis (valence triple-zeta with two sets of polarization functions and a set of diffuse functions) with the PBE1PBE functional was also performed. In case of def2-TZVPPD, the electronic structure of the hydrogen (H) is represented by (5s3p1d)/[3s3p1d], the carbon (C), nitrogen (N), oxygen (O) and fluorine (F) atoms are treated as (12s7p3d1f)/[6s3p3d1f] and the sulfur (S) atom is represented by (15s10p4d1f)/[6s6p4d1f]. The implication of using this basis function is that, for **Eu1** as example, SVP involves 747 primitive gaussian functions and a calculation with TZVPPD deals with 2042 of these functions, resulting in a calculation that is more expensive. The electronic structure of the europium atom was treated by means of the MWB(52)[3] effective core potential (ECP). This ECP includes 52 electrons in the core and the 11 remaining electrons are represented by the optimized

(7s6p5d)/[5s4p3d] valence basis sets. A charge equal to 0 and a singlet multiplicity were attributed to the europium complexes.

Since the PBE1PBE/TZVPPD/MWB52 method provided the geometries of the complexes with the best agreement compared with the crystallographic structure, the spectroscopic properties were calculated using these geometries. The time dependent density functional theory (TD-DFT) method also contained in the ORCA 5.0.3 software [1] was used to calculate the singlet and triplet excited states of the organic ligands present in the complexes. In this step, the CAM-B3LYP/TZVP/MWB52 level of theory was used. In addition, the INDO/S-CIS semiempirical model [4] was also used to estimate the excited states energy of the ligands, with the Eu(III) ion being replaced by a 3e+ point charge. In this procedure, 20 occupied MOs and 20 virtual MOs were included in the INDO configuration interaction single excitation approach.

To evaluate an eventual effect of the DCM solvent on the excited states position, the Conductor-like Polarizable Continuum Model approximation (CPCM), which treats such an effect implicitly, was considered in the calculations performed using the CAM-B3LYP functional with the TZVP basis set. The oscillator strengths and energies of the 25 calculated singlet states were fitted to a Lorentzian function, using a 12 nm arbitrary attributed half-width at half maximum (HWHM) to provide the theoretical absorption spectra of the **Eu1** and **Eu2** complexes.

1.2   Energy transfer (ET) rates

The LUMPAC 1.4.1 software [5] was applied to calculate the ligand-Eu(III) energy transfer (ET) rates using models already applied by us in previous works [2]. With the help of these rates, the ET pathways in a given complex can be proposed. Such models were proposed by Malta [6] and are derived from the Fermi's golden rule. The Hamiltonian involved in energy transfer process considers the contribution from both the direct Coulombic interaction (CI) and the exchange (Ex) mechanisms, yielding the following expressions:

$$W_{ET}^{CI} = \frac{2\pi}{h} \frac{e^2 S_L F}{G(2J+1)} \sum_{\lambda=2,4,6} \Lambda_\lambda \left\langle \psi'J' \left\| U^{(\lambda)} \right\| \psi J \right\rangle^2$$

$$\Lambda_\lambda = 2\Omega_\lambda^{FED} (1-\sigma_1)^2 \left(\frac{1}{R_L^6}\right) + \left\langle r^\lambda \right\rangle^2 \left\langle 3 \left\| C^{(\lambda)} \right\| 3 \right\rangle^2 (1-\sigma_\lambda)^2 \left(\frac{\lambda+1}{\left(R_L^{\lambda+2}\right)^2}\right)$$

$$W_{ET}^{EX} = \frac{8\pi}{3h} \frac{e^2}{R_L^4} \frac{(1-\sigma_0)^2 F}{G(2J+1)} \left\langle \psi'J' \| S \| \psi J \right\rangle^2 \sum_m \left\langle \Psi_{N-1}\Pi \left| \sum_j r_j C_0^{(1)}(j) s_{-m}(j) \right| \Psi_{N-1}\Pi^* \right\rangle^2$$

where *J* is the total angular momentum quantum number of the corresponding excited state of the Eu(III). *G* is the degeneracy of the ligand initial state, in which for a given singlet and triplet state is equal to 1 and 3, respectively.

Important aspects to note in the equations is their dependence on the distance between the energy barycentre of the donor state and the metal centre, known as R_L. This quantity is calculated with help of the atomic orbital coefficients of the *i* atom (c_i) contributing to the ligand state and using the distance from the ith atom to the lanthanide ion ($R_{L,i}$):

$$R_L = \frac{\sum_i c_i^2 R_{L_i}}{\sum_i c_i^2}$$

where c_i is estimated from the TD-DFT results and $R_{L,i}$ are taken from the geometry considered in the TD-DFT calculations.

Another relevant term present in the Eqs. * MERGEFORMAT S1 and * MERGEFORMAT S3 is the energy mismatch spectral overlap F, which depends on the energy difference involving the donor and acceptor energy states of the process of ET (Δ). Since the ligand bandwidth at half-height (γ_L, in s^{-1}) is much larger than the widths of the 4f-4f transitions of Eu(III), the term F is usually calculated using the following equation:

$$F = \frac{1}{h\gamma_L}\sqrt{\frac{ln\,2}{\pi}}\,e^{-\left(\frac{\Delta}{h\gamma_L}\right)^2 ln\,2}$$

The term $(1-\sigma_0)$ contained in Eq. * MERGEFORMAT S3 is approximately calculated by

$$(1-\sigma_0) \approx 0.05\left(\frac{R_{min}}{R_L}\right)^{7/2}$$ and consists of a new improvement recently introduced by Carneiro and workers. [7] The quantity R_{min} is the smallest distance between the atoms of the coordination polyhedron and the metal centre. **Table S1** shows the values of some quantities used to calculate the energy transfer rates for both the CI and Ex mechanisms and supplies a brief description for such quantities.

Table S1:   Values considered of some quantities to estimate the energy transfer rates for both the direct Coulombic interaction (CI) and the exchange (Ex) mechanisms.

Quantity	Description	Value
$\left\langle 3\left\|C^{(\lambda)}\right\|3\right\rangle$	Racah tensor operators	$\left\langle 3\left\|C^{(2)}\right\|3\right\rangle$ = -1.366

		$\left\langle 3\left\|C^{(4)}\right\|3\right\rangle$ = 1.128
		$\left\langle 3\left\|C^{(6)}\right\|3\right\rangle$ = -1.270
$\left\langle r^{\lambda}\right\rangle$	Radial integrals for Eu(III) [8]	$\left\langle r^{2}\right\rangle$ = 0.9175
		$\left\langle r^{4}\right\rangle$ = 2.0200
		$\left\langle r^{6}\right\rangle$ = 9.0390
$\left(1-\sigma_{\lambda}\right)$	Shielding field owing to the *5s* and *5p* filled orbitals [9]	σ_{2} = 0.600
		σ_{4} = 0.139
		σ_{6} = 0.900
S_L	Ligand dipole strength[9]	10^{-35} (e.s.u.)^2 (Singlet donor state) 10^{-40} (e.s.u.)^2 (Triplet donor state)
$\left\langle \Psi_{N-1}\Pi\left\|\sum_j r_j C_0^{(1)}(j)s_{-m}(j)\right\|\Psi_{N-1}\Pi^*\right\rangle^2$	Squared matrix element of the coupled dipole and spin operators[10]	10^{-36} (e.s.u.)^{2}cm^2
γ_L	Ligand bandwidth at half-height	3200 cm^{-1}

The values for the $\left\langle \psi'J'\left\|U^{(\lambda)}\right\|\psi J\right\rangle$ unit operator and $\left\langle \psi'J'\|S\|\psi J\right\rangle$ spin operator matrix elements were taken from the work of Kasprzycka and co-workers [11]. It is important to mention that selection rules are derived from $\left\langle \psi'J'\left\|U^{(\lambda)}\right\|\psi J\right\rangle$ and $\left\langle \psi'J'\|S\|\psi J\right\rangle$, in which $|\Delta J|$ = 2, 4, and 6 for the CI mechanism and $|\Delta J|$ = 0, ±1 (*J* = *J'*= 0 excluded) for the Ex mechanism. These selection rules are associated with the electronic excitation centred on the Ln(III) promoted by ET from the ligands. The excitation from the lowest excited states $^7F_0$ and $^7F_1$ of Eu(III) had thermal population of 0.64 and 0.33 at 300 K [11], respectively. In addition, to include the $^5D_0\leftarrow{}^7F_0$ transition in the calculations, a *J*-mixing between the $^7F_0$ and $^7F_2$ states of 5% was considered, enabling the transition to be allowed by the CI mechanism. The ET rates involving a given excited state of Eu(III) to a ligand excited state were calculated simply by multiply the Boltzmann factor

$\exp\left(-\dfrac{|\Delta|}{k_B T}\right)$ by the corresponding direct ET rates, where T is the RT and k_B stands for the Boltzmann constant.

The Ω_λ^{FED} quantity contained in Eq. * MERGEFORMAT S2 is the intensity parameter related exclusively to the forced electric dipole (FED) mechanism, being derived from the standard Judd-Ofelt theory. Ω_λ^{FED} is calculated by Eq. * MERGEFORMAT S6 considering only the contribution from $B_{\lambda tp}^{FED}$ presents in Eq. * MERGEFORMAT S7.

$$\Omega_\lambda^{calc} = (2\lambda+1) \sum_{t}^{\lambda-1,\lambda+1(odd)} \sum_{p=-t}^{t(all)} \frac{\left|B_{\lambda tp}\right|^2}{(2t+1)}$$

Eq. * MERGEFORMAT S6

$$\begin{aligned}
B_{\lambda tp} &= B_{\lambda tp}^{FED} + B_{\lambda tp}^{DC} \\
&= \frac{2}{\Delta E}\left\langle r^{t+1}\right\rangle \theta(t,\lambda)\gamma_p^t \\
&- \left[\frac{(\lambda+1)(2\lambda+3)}{2\lambda+1}\right]^{1/2} \left\langle r^\lambda\right\rangle (1-\sigma_\lambda)\left\langle 3\left\|C^{(\lambda)}\right\|3\right\rangle \Gamma_p^t \delta_{t,\lambda+1}
\end{aligned}$$

Eq. * MERGEFORMAT S7

The energy difference ΔE presents in Eq. * MERGEFORMAT S7 involves the ground state barycentre and the first excited state of opposite parity ($E_{4f}-E_{nl}$) of the Eu(III) ion, being obtained by the average energy denominator method [12]. $\theta(t,\lambda)$ are numeric factors for the Eu(III) ion and the values estimated by Malta and co-workers [13] using radial integrals of Hartree-Fock calculations are $\theta(1,2)$ = -0.17, $\theta(3,2)$ = 0.345, $\theta(3,4)$ = 0.18, $\theta(5,4)$ = -0.24, $\theta(5,6)$ = -0.24, and $\theta(7,6)$ = 0.24. The $\delta_{t,\lambda+1}$ term is the Kronecker delta function.

The FED and dynamic coupling (DC) mechanisms depend on the γ_p^t (Eq. * MERGEFORMAT S8) and Γ_p^t (Eq. * MERGEFORMAT S9) quantities, respectively. γ_p^t is calculated with the help of the Simple Overlap Model (SOM) [12, 14] that introduces covalency to the

point charge model by including the $\rho_j \left(2\beta_j \right)^{t+1}$ term, where ρ_j corresponds to the overlap between the *4f* orbitals and the valence orbitals of the jth atom directly coordinated to the metal centre. The ρ_j and β_j quantities are calculated by using Eqs. * MERGEFORMAT S10 and * MERGEFORMAT S11.

$$\gamma_p^t = \left(\frac{4\pi}{2t+1} \right)^{\frac{1}{2}} e^2 \sum_j \rho_j \left(2\beta_j \right)^{t+1} \frac{g_j}{R_j^{t+1}} Y_p^{t*} \left(\theta_j, \phi_j \right)$$

$$\Gamma_p^t = \left(\frac{4\pi}{2t+1} \right)^{\frac{1}{2}} \sum_j \frac{\alpha_j}{R_j^{t+1}} Y_p^{t*} \left(\theta_j, \phi_j \right)$$

$$\beta_j = \frac{1}{1 \pm \rho_j}$$

$$\rho_j \approx 0.05 \left(\frac{R_{min}}{R_j} \right)^{3.5}$$

Both γ_p^t and Γ_p^t depend on the $\left(R_j, \theta_j, \phi_j \right)$ spherical coordinates of the jth atom of the coordination polyhedron of the compound and R_{min} is the smallest R_j distance. These coordinates are useful to calculate the complex conjugate of the spherical harmonics (Y_p^{t*}).

The charge factor (g_j) and the polarizability (α_j) were estimated by the LUMPAC software [5] applying the *QDC* model [15]. This model postulates that each charge factor is calculated by using the Zero Differential Overlap (ZDO) electronic density (q_j) and each polarizability is calculated by

using the electrophilic superdelocalizability (SE_j). In addition, g and α are obtained with the help of the adjustable parameters Q, D, and C to reproduce the experimental values of Ω_λ.

$$g_j = Q.q_j$$

Eq. * MERGEFORMAT S12

$$\alpha_j = SE_j \cdot D + C$$

Eq. * MERGEFORMAT S13

The atomic orbitals coefficients (c) involved in the occupied MOs are used to calculate the ZDO charges and the superdelocalizabilities, as shown by Eqs. * MERGEFORMAT S14 and * MERGEFORMAT S15. To calculate such quantities, wavefunctions obtained using the RM1 semipirical quantum mechanical model [16] implemented in the MOPAC program [17] were considered.

$$q_j = 2\sum_{i'}^{occ.}\sum_{p}\left|c_{pi'}^j\right|^2$$

Eq. * MERGEFORMAT S14

$$SE_j = 2\sum_{i'}^{occ.}\sum_{p}\sum_{q}\frac{c_{pi'}^j c_{qi'}^j}{\varepsilon_{i'}}$$

Eq. * MERGEFORMAT S15

1.3   Radiative emission rate (A_{Rad}) and photoluminescence quantum yield (PLQY)

The theoretical radiative emission rate (A_{Rad}) due to the electric dipole mechanism was calculated using the intensity parameters obtained from the QDC model. On the other hand, the magnetic dipole strength (S_{md}) of the ${}^5D_0 \rightarrow {}^7F_1$ transition assumed the theoretical value of

9.6×10^{-42} esu^{2}cm^2 [18] in the calculation. When the metal centre is the Eu(III) ion, A_{Rad} is then calculated by Eq. * MERGEFORMAT S16.

$$A_{Rad} = \frac{32e^2\pi^3\chi}{3h(2J+1)} \sum_{\lambda=2,4,6} \nu[^5D_0 \rightarrow {}^7F_{J=\lambda}]^3 \Omega_\lambda \left| \left\langle {}^5D_0 \left\| U^{(\lambda)} \right\| {}^7F_{J=\lambda} \right\rangle \right|^2 +$$
$$\frac{32\pi^3n^3\nu[^5D_0 \rightarrow {}^7F_1]^3}{3h} S_{md}$$

where the Lorentz local-field correction (χ) depends on the n refractive index and is estimated by the expression $\chi = n(n^2+2)^2/9$. $\nu[^5D_0 \rightarrow {}^7F_J]$ is the energy of the barycenter of the respective transition ($^5D_0 \rightarrow {}^7F_2$, $^5D_0 \rightarrow {}^7F_4$, and $^5D_0 \rightarrow {}^7F_6$). A refractive index of 1.424 due to the DCM solvent was considered.

The theoretical PLQY (Q_{Eu}^L) is defined as the number of emitted photons by the lanthanide ion to the number of absorbed photons by the ligand and is calculated by the Eq. * MERGEFORMAT S17.

$$Q_{Eu}^L = \frac{A_{rad}\eta_{^5D_0}}{\varphi\eta_{S_0}}$$

where φ is the absorption rate (s^{-1}) from the fundamental singlet (S$_0$) to a given excited singlet of the ligand. It is needed to know the energetic population of the absorber (η_{S_0}) and emitting ($\eta_{^5D_0}$) states of Eu (III) to calculate the theoretical Q_{Eu}^L value. In this context, the normalized population of each state included in the modeling of the energy transfer is obtained by using a system of equations. The energetic population of a given a state in the steady-state condition is generically expressed by:

$$\frac{d\eta_a}{dt} = -\sum_{a \neq b} W_{ba}\eta_b + \sum_{a \neq b} W_{ab}\eta_a = 0$$

where W_{ab} is the energy transfer rate from the *a* to the *b* state, and vice-versa.

2.   OLEDs Device configuration

2.1.   Single-EML Device configuration of **Eu1**:

Device 1：ITO/HAT-CN (23 nm)/HAT-CN (0.3 wt%): TAPC (70 nm)/**Eu1**(2 wt%): CzSi (10 nm)/Tm3PyP26PyB (60 nm)/LiF (1 nm)/Al (200 nm)

Device 2 : ITO/HAT-CN (23 nm)/HAT-CN (0.3 wt%): TAPC (70 nm)/**Eu1**(3 wt%): CzSi (10 nm)/Tm3PyP26PyB (60 nm)/LiF (1 nm)/Al (200 nm)

Device 3 : ITO/HAT-CN (23 nm)/HAT-CN (0.3 wt%): TAPC (70 nm)/**Eu1**(4 wt%): CzSi (10 nm)/Tm3PyP26PyB (60 nm)/LiF (1 nm)/Al (200 nm)

Device 4 : ITO/HAT-CN (23 nm)/HAT-CN (0.3 wt%): TAPC (70 nm)/**Eu1**(5 wt%): CzSi (10 nm)/Tm3PyP26PyB (60 nm)/LiF (1 nm)/Al (200 nm)

Device 5 : ITO/HAT-CN (23 nm)/HAT-CN (0.3 wt%): TAPC (70 nm)/**Eu1**(6 wt%): CzSi (10 nm)/Tm3PyP26PyB (60 nm)/LiF (1 nm)/Al (200 nm)

2.2.   **Double-EML Device configuration of Eu1**:

Device 6 : ITO/HAT-CN (23 nm)/HAT-CN (0.3 wt%): TAPC (70 nm)/ **Eu1** (2 wt%):TcTa (10 nm)/ **Eu1** (2 wt%):CzSi (10 nm)/Tm3PyP26PyB (60 nm)/LiF (1 nm)/Al (200 nm)

Device 7 ： ITO/HAT-CN (23 nm)/HAT-CN (0.3 wt%): TAPC (70 nm)/ **Eu1** (3 wt%):TcTa (10 nm)/

Eu1 (3 wt%):CzSi (10 nm)/Tm3PyP26PyB (60 nm)/LiF (1 nm)/Al (200 nm)

Device 8 ： ITO/HAT-CN (23 nm)/HAT-CN (0.3 wt%): TAPC (70 nm)/ **Eu1** (4 wt%):TcTa (10 nm)/

Eu1 (4 wt%):CzSi (10 nm)/Tm3PyP26PyB (60 nm)/LiF (1 nm)/Al (200 nm)

Device 9 ： ITO/HAT-CN (23 nm)/HAT-CN (0.3 wt%): TAPC (70 nm)/ **Eu1** (5 wt%):TcTa (10 nm)/

Eu1 (5 wt%):CzSi (10 nm)/Tm3PyP26PyB (60 nm)/LiF (1 nm)/Al (200 nm)

Device 10 ： ITO/HAT-CN (23 nm)/HAT-CN (0.3 wt%): TAPC (70 nm)/ **Eu1** (6 wt%):TcTa (10

nm)/ **Eu1** (6 wt%):CzSi (10 nm)/Tm3PyP26PyB (60 nm)/LiF (1 nm)/Al (200 nm)

2.3. Single-EML Device configuration of Eu2:

Device 1 ： ITO/HAT-CN (23 nm)/HAT-CN (0.3 wt%): TAPC (70 nm)/ **Eu2** (**1 wt%**): 26DCzPPy

(10 nm)/Tm3PyP26PyB (60 nm)/LiF (1 nm)/Al (200 nm)

Device 2 ： ITO/HAT-CN (23 nm)/HAT-CN (0.3 wt%): TAPC (70 nm)/ **Eu2** (**2 wt%**): 26DCzPPy

(10 nm)/Tm3PyP26PyB (60 nm)/LiF (1 nm)/Al (200 nm)

Device 3 ： ITO/HAT-CN (23 nm)/HAT-CN (0.3 wt%): TAPC (70 nm)/ **Eu2** (**4 wt%**): 26DCzPPy

(10 nm)/Tm3PyP26PyB (60 nm)/LiF (1 nm)/Al (200 nm)

Device 4 ： ITO/HAT-CN (23 nm)/HAT-CN (0.3 wt%): TAPC (70 nm)/ **Eu2** (**6 wt%**): 26DCzPPy

(10 nm)/Tm3PyP26PyB (60 nm)/LiF (1 nm)/Al (200 nm)

Device 5 ： ITO/HAT-CN (23 nm)/HAT-CN (0.3 wt%): TAPC (70 nm)/ **Eu2** (**8 wt%**): 26DCzPPy

(10 nm)/Tm3PyP26PyB (60 nm)/LiF (1 nm)/Al (200 nm)

2.4. Double-EML Device configuration of Eu2:

Device 6： ITO/HAT-CN (23 nm)/HAT-CN (0.3 wt%): TAPC (70 nm)/ **Eu2** (**1 wt%**):TcTa (10 nm)/

Eu2 (**1 wt%**):26DCzPPy (10 nm)/Tm3PyP26PyB (60 nm)/LiF (1 nm)/Al (200 nm)

Device 7： ITO/HAT-CN (23 nm)/HAT-CN (0.3 wt%): TAPC (70 nm)/ **Eu2** (**2 wt%**):TcTa (10 nm)/

Eu2 (**2 wt%**):26DCzPPy (10 nm)/Tm3PyP26PyB (60 nm)/LiF (1 nm)/Al (200 nm)

Device 8： ITO/HAT-CN (23 nm)/HAT-CN (0.3 wt%): TAPC (70 nm)/ **Eu2** (**4 wt%**):TcTa (10 nm)/

Eu2 (**4 wt%**):26DCzPPy (10 nm)/Tm3PyP26PyB (60 nm)/LiF (1 nm)/Al (200 nm)

Device 9： ITO/HAT-CN (23 nm)/HAT-CN (0.3 wt%): TAPC (70 nm)/ **Eu2** (**6 wt%**):TcTa (10 nm)/

Eu2 (**6 wt%**):26DCzPPy (10 nm)/Tm3PyP26PyB (60 nm)/LiF (1 nm)/Al (200 nm)

Device 10： ITO/HAT-CN (23 nm)/HAT-CN (0.3 wt%): TAPC (70 nm)/ **Eu2** (**8 wt%**):TcTa (10

nm)/ **Eu2** (**8 wt%**):26DCzPPy (10 nm)/Tm3PyP26PyB (60 nm)/LiF (1 nm)/Al (200 nm)

Table S2: Crystal data and structure refinement for europium complexes.

	Eu1	Eu2
Empirical formula	$C_{25}H_{19}N_3O_6EuSF_9$	$C_{25}H_{10}N_3O_6F_{18}SEu$
Formula weight	812.45	974.38
CCDC Number	2178685	2178686
Temperature/K	293(2)	297(2)
Crystal system	monoclinic	triclinic
Space group	$P2_1/n$	P-1
a/Å	10.870(2)	9.7200(19)
b/Å	13.970(3)	12.770(3)
c/Å	20.690(4)	14.300(3)
α/°	90	82.80(3)
β/°	93.30(3)	76.70(3)
γ/°	90	83.90(3)
Volume/Å^3	3136.6(11)	1708.2(6)
Z	4	2
ρ_{calc}g/cm^3	1.720	1.894
μ/mm^{-1}	2.161	2.038
F(000)	1592.0	940.0
Crystal size/mm^3	0.200 × 0.200 × 0.200	0.200 × 0.200 × 0.200
Radiation	MoKα (λ = 0.71073)	MoKα (λ = 0.71073)
2Θ range for data collection/°	4.904 to 54.998	5.18 to 59.998
Index ranges	-14 ≤ h ≤ 14, -15 ≤ k ≤ 18, -26 ≤ l ≤ 26	-13 ≤ h ≤ 13, -17 ≤ k ≤ 17, -20 ≤ l ≤ 20
Reflections collected	27483	19762
Independent reflections	7166 [R_{int} = 0.0395, R_{sigma} = 0.0250]	9917 [R_{int} = 0.0384, R_{sigma} = 0.0379]
Completeness to θ = 25.242°	99.7 %	99.4 %
Absorption correction	Semi-empirical from equivalents	Semi-empirical from equivalents
Max. and min. transmission	0.99 and 0.7	0.6 and 0.6

Final R indexes [I>=2σ (I)]	$R_1 = 0.0376$, $wR_2 = 0.0948$	$R_1 = 0.0484$, $wR_2 = 0.1256$
Final R indexes [all data]	$R_1 = 0.0464$, $wR_2 = 0.1015$	$R_1 = 0.0628$, $wR_2 = 0.1379$
Largest diff. peak/hole /e Å^{-3}	1.09/-0.73	1.10/-0.80
Refinement method	Full-matrix least-squares on F^2	Full-matrix least-squares on F^2
Extinction coefficient	0.00042(16)	0.0048(7)

Table S3:   Continuous shape measures (CShMs) of the crystallographic coordination polyhedron for the Eu(III) in **Eu1** and **Eu2**.

Shape	Symmetry	CShMs Eu-1	CShMs Eu-2
Octagon	D_{8h}	30.785	32.208
Heptagonal pyramid	C_{7v}	23.592	24.296
Hexagonal bipyramid	D_{6h}	14.857	15.095
Cube	O_h	8.052	8.910
Square antiprism	D_{4d}	1.552	2.993
Triangular dodecahedron	D_{2d}	0.629	0.695
Johnson - Gyrobifastigium (J26)	D_{2d}	15.640	14.830
Johnson - Elongated triangular bipyramid (J14)	D_{3h}	29.034	28.377
Johnson - Biaugmented trigonal prism (J50)	C_{2v}	2.720	3.021
Biaugmented trigonal prism	C_{2v}	1.906	2.217
Snub disphenoid (J84)	D_{2d}	3.493	3.223
Triakis tetrahedron	T_d	8.760	9.567
Elongated trigonal bipyramid	D_{3h}	23.705	23.962

Table S4: Root mean square deviation value (RMSD, in Å) between the X-ray geometry for **Eu1** and **Eu2** and the corresponding geometries optimized with DFT methods. The mean of the lanthanide-ligand atom distances is represented by **d**.

Compound	Method	RMSD (all atoms)	RMSD (coordination polyhedron)	d_{Eu-O}	d_{Eu-N}
Eu1	X-ray	-	-	2.371	2.574
	B3LYP/SVP	0.7206	0.2784	2.409	2.695
	B3LYP/TZVP	0.6593	0.2108	2.420	2.683
	PBE1PBE/SVP	0.6341	0.2897	2.394	2.665
	PBE1PBE/TZVP	0.6486	0.2440	2.401	2.654
	PBE1PBE/TZVPPD	0.6148	0.2204	2.396	2.663
Eu2	X-ray	-	-	2.383	2.554
	B3LYP/SVP	0.9769	0.3448	2.413	2.674
	B3LYP/TZVP	0.6324	0.2121	2.430	2.653
	PBE1PBE/SVP	0.6383	0.2167	2.397	2.633
	PBE1PBE/TZVP	0.7269	0.2713	2.408	2.623
	PBE1PBE/TZVPPD	0.4957	0.1471	2.402	2.644

Table S5: Electronic transitions calculated at the CAM-B3LYP/TZVPPD/MWB52 level of theory for the most intense bands of **Eu1** and **Eu2**.

	Wavelength	Oscillator strength	Major Contribution	Total
Eu1	235.63 nm	1.0048	HOMO→**LUMO+3** (13.50%) HOMO-1→LUMO+1 (12.35%) HOMO-3→LUMO+1 (11.11%) HOMO-1→LUMO+2 (10.18%) HOMO→LUMO+2 (8.93%) **HOMO-2→LUMO** (8.00%)	64.06%
	265.59 nm	0.3677	**HOMO-2→LUMO** (63.22%) HOMO→**LUMO** (5.55%)	68.77%
Eu2	244.96 nm	0.6539	HOMO-1→LUMO+2 (32.92%) HOMO-3→LUMO+1 (21.84%) HOMO→LUMO (8.18%) **HOMO-2→LUMO** (7.23%) HOMO-4→LUMO+2 (5.45%) HOMO-3→LUMO+2 (5.28%)	80.90%
	268.30 nm	0.3660	**HOMO→LUMO** (67.35%) **HOMO**→LUMO+4 (5.97%)	73.32%

MOs centered on the ancillary ligand are highlighted in bold.

Table S6: ZDO electronic density (q), electrophilic superdelocalizability (SE), charge factor (g) and polarizability (α) for each atom directly coordinated to Eu(III) in **Eu1** and **Eu2**. These properties were estimated with the help of the wavefunction obtained with the RM1 model, considering the PBE1PBE/TZVPPD/MWB52 geometry.

Eu1	QDC parameters		
	$Q = 0.1870$ au^{-1}; $D = 43.1802$ au^{-1}·Å^3; $C = 18.4161$ Å^3		
	$D/C = 2.34$ au^{-1}		
Ligand atom	q (au)	SE (au)	g	α (Å^3)
O(tfac 1)	6.3319	-0.4264	1.1840	0.0054
O(tfac 1)	6.3245	-0.3928	1.1826	1.4569
O(tfac 2)	6.3315	-0.2577	1.1839	7.2900
O(tfac 2)	6.3342	-0.3623	1.1844	2.7698
O(tfac 3)	6.3501	-0.2643	1.1874	7.0048
O(tfac 3)	6.3117	-0.2830	1.1802	6.1971
N(TB-Im)	5.2146	-0.3584	0.9751	2.9412
N(TB-Im)	5.1456	-0.3639	0.9622	2.7041

$\Omega_2^{FED} = 0.0641 \times 10^{-20}$ cm^2; $\Omega_4^{FED} = 0.2734 \times 10^{-20}$ cm^2 and $\Omega_6^{FED} = 0.4986 \times 10^{-20}$ cm^2

Eu2	QDC parameters		
	$Q = 0.0543$ au^{-1}; $D = 31.0122$ au^{-1}·Å^3; $C = 13.3722$ Å^3		
	$D/C = 2.32$ au^{-1}		
Ligand atom	q (au)	SE (au)	g	α (Å^3)
O(hfac 1)	6.3156	-0.4018	0.3431	0.9118
O(hfac 1)	6.3153	-0.3533	0.3431	2.4147
O(hfac 2)	6.3059	-0.3812	0.3426	1.5489
O(hfac 2)	6.3154	-0.4233	0.3431	0.2460

O(hfac 3)	6.3079	-0.2336	0.3427	6.1267
O(hfac 3)	6.3117	-0.1782	0.3429	7.8458
N(TB-Im)	5.2251	-0.2695	0.2839	5.0137
N(TB-Im)	5.1602	-0.3402	0.2804	2.8204
	$\Omega_2{}^{FED} = 0.0064\times10^{-20}$ cm^2; $\Omega_4{}^{FED} = 0.0211\times10^{-20}$ cm^2 and $\Omega_6{}^{FED} = 0.0481\times10^{-20}$ cm^2			

Table S7: Distance between the energy barycenter of the lowest singlet and triplet donor state and the metal center and corresponding energy, with and without the effect of the DCM solvent.

Without the Effect of Solvent					
Complex	**DFT //** **TD-DFT**	**S$_1$**		**T$_1$**	
		R_L (Å)	Energy (cm^{-1})	R_L (Å)	Energy (cm^{-1})
Eu1	B3LYP/SVP // CAM-B3LYP/TZVP	3.6808	34615.8	3.6891	23800.6
	B3LYP/TZVP // CAM-B3LYP/TZVP	3.6585	34838.1	3.6202	24021.4
	PBE1PBE/SVP // CAM-B3LYP/TZVP	3.7199	34817.4	3.7319	24174.7
	PBE1PBE/TZVP // CAM-B3LYP/TZVP	3.6539	35088.5	3.6321	24417.7
	PBE1PBE/TZVPPD // CAM-B3LYP/TZVPPD	3.6215	35108.7	3.5591	24335.0
	PBE1PBE/TZVPPD // INDO/S-CIS	4.3659	31546.9	4.0886	14550.3
Eu2	B3LYP/SVP // CAM-B3LYP/TZVP	3.7829	33938.5	3.8170	22057.8
	B3LYP/TZVP // CAM-B3LYP/TZVP	3.5123	33856.5	3.6950	22250.1
	PBE1PBE/SVP // CAM-B3LYP/TZVP	3.6465	34341.7	3.7096	22326.0
	PBE1PBE/TZVP // CAM-B3LYP/TZVP	3.7207	34627.4	3.6767	22553.4

Compound	DFT // TDDFT	R_L (Å)	Energy (cm^{-1})	R_L (Å)	Energy (cm^{-1})
	PBE1PBE/TZVPPD // CAM-B3LYP/TZVPPD	3.3973	34273.3	3.2189	22473.6
	PBE1PBE/TZVPPD // INDO/S-CIS	4.0463	30899.9	3.9910	14424.1

With the Effect of Solvent

Compound	DFT // TDDFT	S$_1$		T$_1$	
		R_L (Å)	Energy (cm^{-1})	R_L (Å)	Energy (cm^{-1})
Eu1	B3LYP/SVP // CAM-B3LYP/TZVP	3.7733	35041.8	3.5958	23773.2
	B3LYP/TZVP // CAM-B3LYP/TZVP	3.7381	35250.3	3.7381	23985.0
	PBE1PBE/SVP // CAM-B3LYP/TZVP	3.8043	35283.8	3.6245	24154.8
	PBE1PBE/TZVP // CAM-B3LYP/TZVP	3.7259	35500.2	3.7338	24385.6
	PBE1PBE/TZVPPD // CAM-B3LYP/TZVPPD	3.4485	35475.1	3.6026	24326.3
Eu2	B3LYP/SVP // CAM-B3LYP/TZVP	3.3764	34464.5	3.5475	21739.2
	B3LYP/TZVP // CAM-B3LYP/TZVP	3.5747	34385.5	3.5104	21918.9
	PBE1PBE/SVP // CAM-B3LYP/TZVP	3.4473	34737.1	3.6512	22073.7
	PBE1PBE/TZVP // CAM-B3LYP/TZVP	3.3161	34947.9	3.5651	22253.4
	PBE1PBE/TZVPPD // CAM-B3LYP/TZVPPD	3.2805	34505.5	3.2957	22252.4

Table S8: Energy transfer rates estimated using the Malta's model [7] considering the excited states calculated at the TD-DFT CAM-B3LYP/TZVPPD/MWB52 level of theory using the PBE1PBE/ TZVPPD/MWB52 geometry. The effect of the DCM solvent was implicitly included in the calculations.

	Donor	Acceptor	W_{ET}^{CI} (s^{-1})	W_{ET}^{EX} (s^{-1})	W_{BET} (s^{-1})
Eu1	S$_1$	$^7F_0 \rightarrow ^5D_0$	8.86×10^{-3}	0.0	1.19×10^{-40}
		$^7F_0 \rightarrow ^5D_1$	0.0	1.93×10^1	1.06×10^{-33}
		$^7F_0 \rightarrow ^5L_6$	3.10×10^3	0.0	2.24×10^{-18}
		$^7F_0 \rightarrow ^5G_6$	4.39×10^3	0.0	2.97×10^{-15}
		$^7F_0 \rightarrow ^5D_4$	7.30×10^4	0.0	2.70×10^{-12}
		$^7F_1 \rightarrow ^5D_0$	0.0	1.03×10^0	2.32×10^{-39}
		$^7F_1 \rightarrow ^5D_1$	1.09×10^1	4.60×10^{-3}	1.01×10^{-34}
		$^7F_1 \rightarrow ^5D_2$	0.0	6.85×10^1	8.27×10^{-29}
		$^7F_1 \rightarrow ^5D_3$	1.54×10^4	0.0	1.78×10^{-20}
		$^7F_1 \rightarrow ^5L_6$	5.73×10^2	0.0	6.96×10^{-20}
		$^7F_1 \rightarrow ^5L_7$	3.83×10^3	0.0	6.56×10^{-17}
		$^7F_1 \rightarrow ^5G_2$	0.0	4.12×10^5	8.34×10^{-15}
		$^7F_1 \rightarrow ^5G_3$	1.73×10^5	0.0	1.06×10^{-14}
		$^7F_1 \rightarrow ^5G_6$	1.58×10^3	0.0	1.80×10^{-16}
		$^7F_1 \rightarrow ^5G_5$	7.56×10^3	0.0	9.07×10^{-16}
	T$_1$	$^7F_0 \rightarrow ^5D_0$	2.14×10^0	0.0	$4.80e^{-15}$
		$^7F_0 \rightarrow ^5D_1$	0.0	9.71×10^7	8.90×10^{-4}
		$^7F_0 \rightarrow ^5L_6$	5.67×10^0	0.0	6.82×10^2
		$^7F_0 \rightarrow ^5G_6$	9.95×10^{-1}	0.0	1.12×10^5
		$^7F_0 \rightarrow ^5D_4$	4.29×10^0	0.0	2.64×10^7
		$^7F_1 \rightarrow ^5D_0$	0.0	1.12×10^8	4.23×10^{-8}

		$^7F_1 \rightarrow \,^5D_1$	3.58×10^2	3.98×10^4	6.19×10^{-8}
		$^7F_1 \rightarrow \,^5D_2$	0.00	1.63×10^7	3.28×10^0
		$^7F_1 \rightarrow \,^5D_3$	2.07×10^2	0.0	3.99×10^1
		$^7F_1 \rightarrow \,^5L_6$	1.81×10^0	0.0	3.65×10^1
		$^7F_1 \rightarrow \,^5L_7$	2.67×10^0	0.0	7.61×10^3
		$^7F_1 \rightarrow \,^5G_2$	0.0	7.45×10^7	2.51×10^{11}
		$^7F_1 \rightarrow \,^5G_3$	8.43×10^1	0.0	8.56×10^5
		$^7F_1 \rightarrow \,^5G_6$	6.19×10^{-1}	0.0	1.17×10^4
		$^7F_1 \rightarrow \,^5G_5$	2.77×10^0	0.0	5.53×10^4
Eu2	S_1	$^7F_0 \rightarrow \,^5D_0$	8.13×10^{-2}	0.0	1.15×10^{-37}
		$^7F_0 \rightarrow \,^5D_1$	0.0	2.56×10^2	1.48×10^{-30}
		$^7F_0 \rightarrow \,^5L_6$	6.97×10^3	0.0	5.27×10^{-16}
		$^7F_0 \rightarrow \,^5G_6$	8.23×10^3	0.0	5.83×10^{-13}
		$^7F_0 \rightarrow \,^5D_4$	2.58×10^5	0.0	9.98×10^{-10}
		$^7F_1 \rightarrow \,^5D_0$	0.00	4.12×10^1	5.81×10^{-35}
		$^7F_1 \rightarrow \,^5D_1$	1.80×10^2	1.36×10^{-1}	1.04×10^{-30}
		$^7F_1 \rightarrow \,^5D_2$	0.0	1.32×10^3	9.89×10^{-25}
		$^7F_1 \rightarrow \,^5D_3$	1.01×10^5	0.0	7.30×10^{-17}
		$^7F_1 \rightarrow \,^5L_6$	2.14×10^3	0.0	1.62×10^{-16}
		$^7F_1 \rightarrow \,^5L_7$	1.19×10^4	0.0	1.27×10^{-13}
		$^7F_1 \rightarrow \,^5G_2$	0.0	3.33×10^6	4.20×10^{-11}
		$^7F_1 \rightarrow \,^5G_3$	7.77×10^5	0.0	2.95×10^{-11}
		$^7F_1 \rightarrow \,^5G_6$	4.59×10^3	0.0	3.25×10^{-13}
		$^7F_1 \rightarrow \,^5G_5$	3.12×10^4	0.0	2.33×10^{-12}
	T_1	$^7F_0 \rightarrow \,^5D_0$	1.44×10^1	0.0	6.76×10^{-10}
		$^7F_0 \rightarrow \,^5D_1$	0.0	8.29×10^8	1.59×10^2
		$^7F_0 \rightarrow \,^5L_6$	2.95×10^0	0.0	7.40×10^6
		$^7F_0 \rightarrow \,^5G_6$	3.51×10^{-1}	0.0	8.26×10^8
		$^7F_0 \rightarrow \,^5D_4$	2.91×10^0	0.0	3.74×10^{11}
		$^7F_1 \rightarrow \,^5D_0$	0.0	2.16×10^9	1.01×10^{-1}
		$^7F_1 \rightarrow \,^5D_1$	1.97×10^3	4.40×10^5	8.46×10^{-2}

		$^7F_1 \rightarrow ^5D_2$	0.0	8.19×10^7	2.05×10^6
		$^7F_1 \rightarrow ^5D_3$	2.10×10^2	0.0	5.03×10^6
		$^7F_1 \rightarrow ^5L_6$	9.04×10^{-1}	0.0	2.27×10^6
		$^7F_1 \rightarrow ^5L_7$	9.59×10^{-1}	0.0	3.40×10^8
		$^7F_1 \rightarrow ^5G_2$	0.0	7.73×10^7	3.24×10^{16}
		$^7F_1 \rightarrow ^5G_3$	4.20×10^1	0.0	5.31×10^{10}
		$^7F_1 \rightarrow ^5G_6$	1.96×10^{-1}	0.0	4.61×10^8
		$^7F_1 \rightarrow ^5G_5$	1.32×10^0	0.0	3.27×10^9
	T_4	$^7F_0 \rightarrow ^5D_0$	1.67×10^{-1}	0.0	5.45×10^{-22}
		$^7F_0 \rightarrow ^5D_1$	0.0	3.24×10^7	4.31×10^{-10}
		$^7F_0 \rightarrow ^5L_6$	7.41×10^0	0.0	1.29×10^{-3}
		$^7F_0 \rightarrow ^5G_6$	2.20×10^0	0.0	3.60×10^{-1}
		$^7F_0 \rightarrow ^5D_4$	2.82×10^1	0.0	2.52×10^2
		$^7F_1 \rightarrow ^5D_0$	0.0	2.79×10^7	9.07×10^{-14}
		$^7F_1 \rightarrow ^5D_1$	6.93×10^1	1.72×10^4	2.30×10^{-13}
		$^7F_1 \rightarrow ^5D_2$	0.0	1.54×10^7	2.67×10^{-5}
		$^7F_1 \rightarrow ^5D_3$	2.25×10^2	0.0	3.75×10^{-4}
		$^7F_1 \rightarrow ^5L_6$	2.27×10^0	0.0	3.97×10^{-4}
		$^7F_1 \rightarrow ^5L_7$	4.67×10^0	0.0	1.15×10^{-1}
		$^7F_1 \rightarrow ^5G_2$	0.0	3.37×10^8	9.80×10^6
		$^7F_1 \rightarrow ^5G_3$	1.94×10^2	0.0	1.70×10^1
		$^7F_1 \rightarrow ^5G_6$	1.23×10^0	0.0	2.01×10^{-1}
		$^7F_1 \rightarrow ^5G_5$	7.86×10^0	0.0	1.36×10^0

Table S9: Key EL properties of the double-EML devices of **Eu1** and **Eu2** operating at J = 10 mA/cm².

Doping concentration	$V_{turn-on}$ (V)	B^a (cd/m²)	η_c^b (cd/A)	η_p^c (lm/W)	EQE (%)	$CIE_{x,y}^g$
Eu1						
2 wt% (Device 6)	4.4	45.31	0.074	0.047	0.052%	(0.257,0.238)
3 wt% (Device 7)	4.2	37.06	0.066	0.046	0.047%	(0.280,0.239)
4 wt% (Device 8)	4.2	95.91	0.086	0.049	0.062%	(0.254,0.227)
5 wt% (Device 9)	4.2	38.98	0.058	0.038	0.047%	(0.247,0.201)
6 wt% (Device 10)	4.8	28.50	0.064	0.039	0.042%	(0.273,0.276)
Eu2						
2 wt% (Device 6)	3.7	356.8	0.260	0.220	0.200%	(0.285,0.174)
3 wt% (Device 7)	3.7	250.8	0.217	0.184	0.171%	(0.288,0.172)
4 wt% (Device 8)	4.1	160.5	0.214	0.164	0.143%	(0.378,0.259)
6 wt% (Device 9)	4.3	155.9	0.244	0.178	0.155%	(0.420,0.297)
8 wt% (Device 10)	4.3	145.6	0.257	0.188	0.160%	(0.416,0.296)
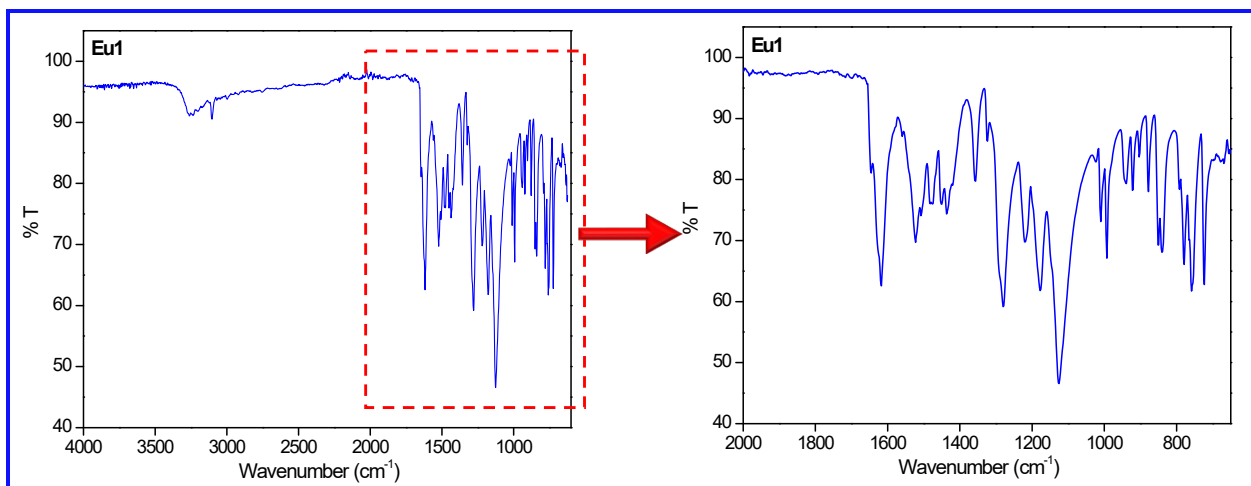
Fig. S1: FT-IR spectrum of **Eu1** with their expansion in the region between 2000 and 650 cm^{-1}.
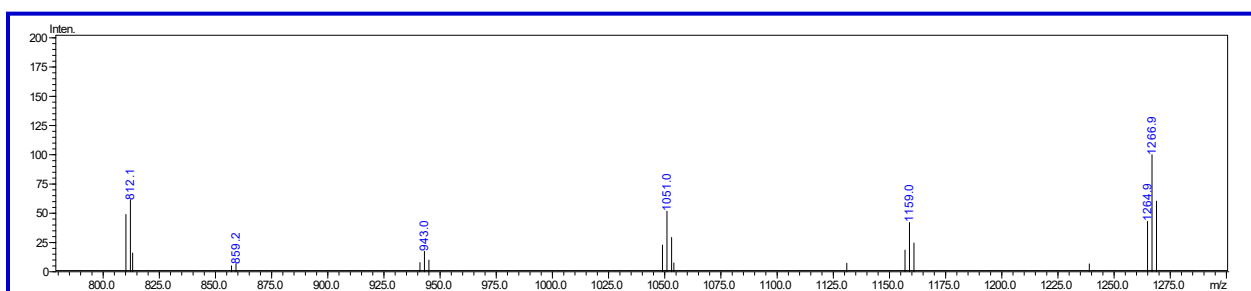
Fig. S2: ESI-MS spectrum of **Eu1**.
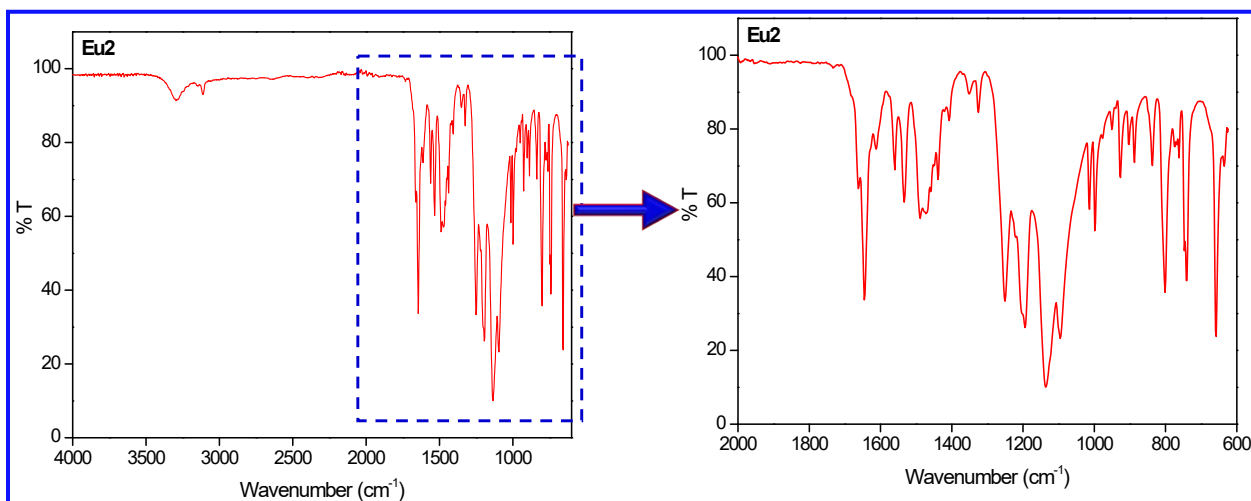
Fig. S3: FT-IR spectrum of **Eu2** with their expansion in the region between 2000 and 650 cm^{-1}.
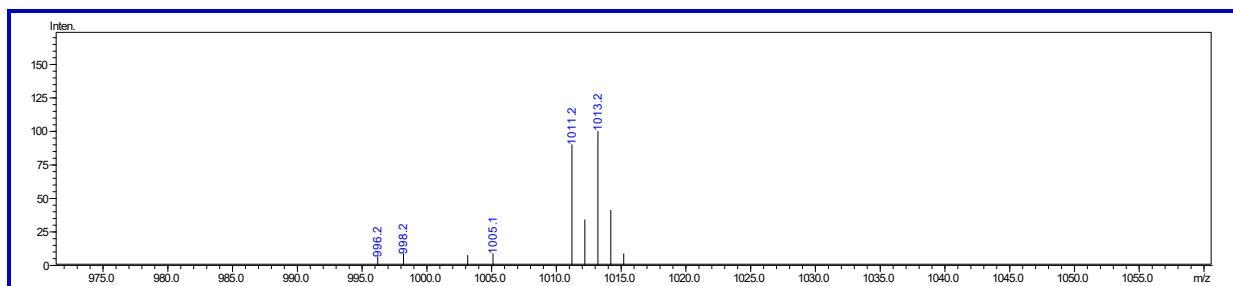
Fig. S4: ESI-MS spectrum of **Eu2**.
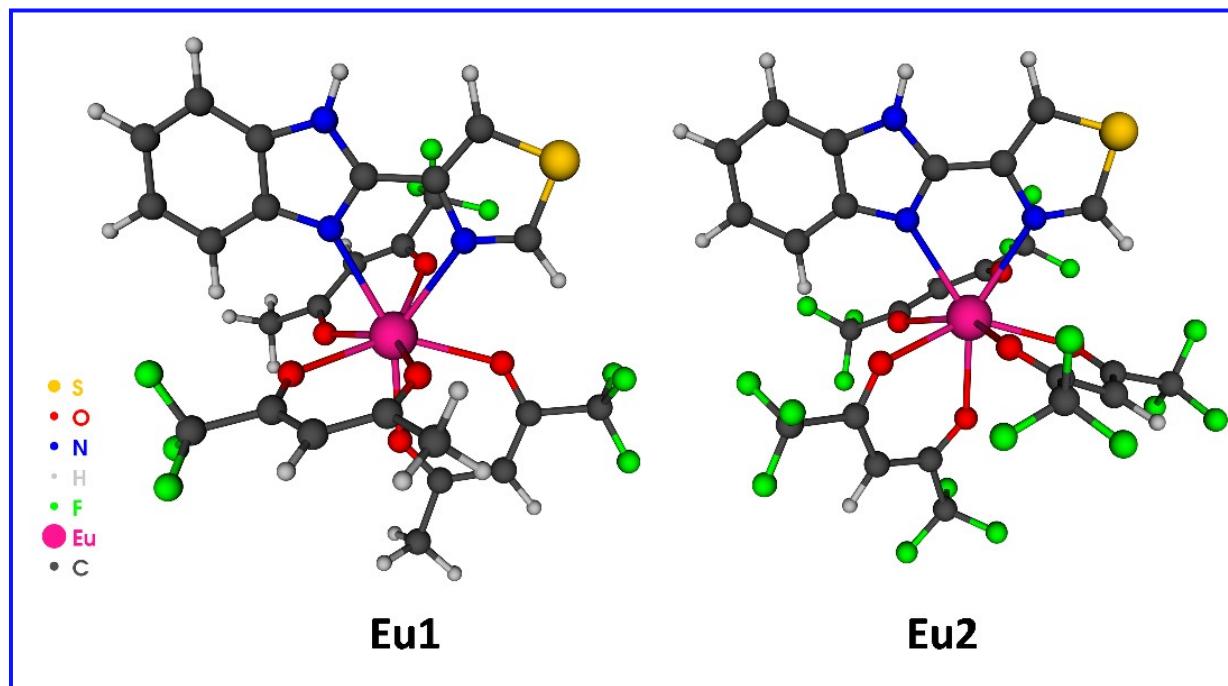
Fig. S5: Geometry of **Eu1** and **Eu2** optimized at the PBE1PBE/TZVPPD/MWB52 level of theory.

Eu1

33%

29%

20 %

246.3 nm

89%

269.0 nm

Eu2

48%

254.4 nm

35%

73%

270.7 nm

12%
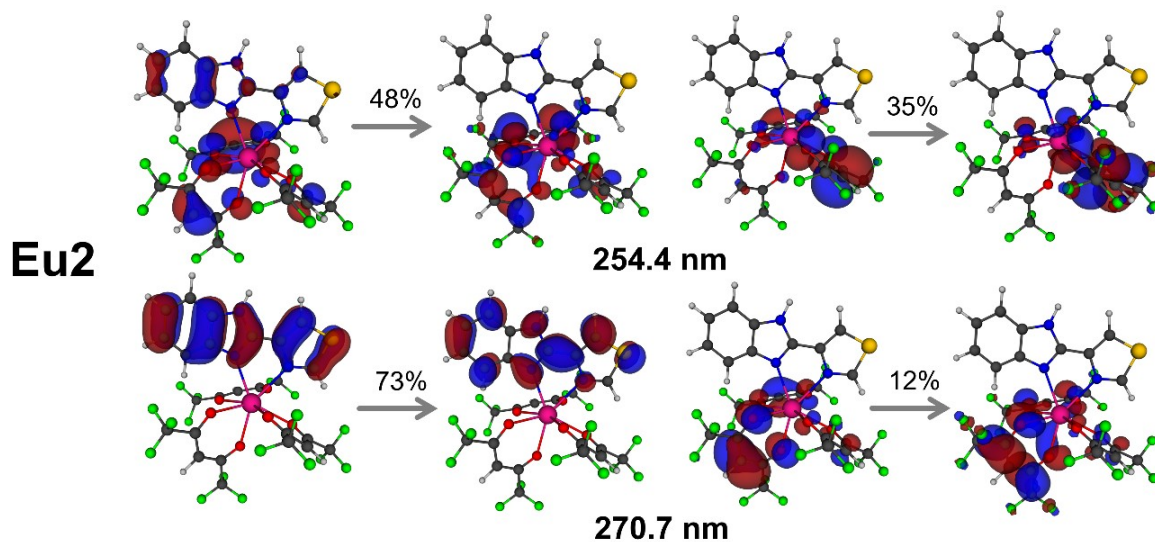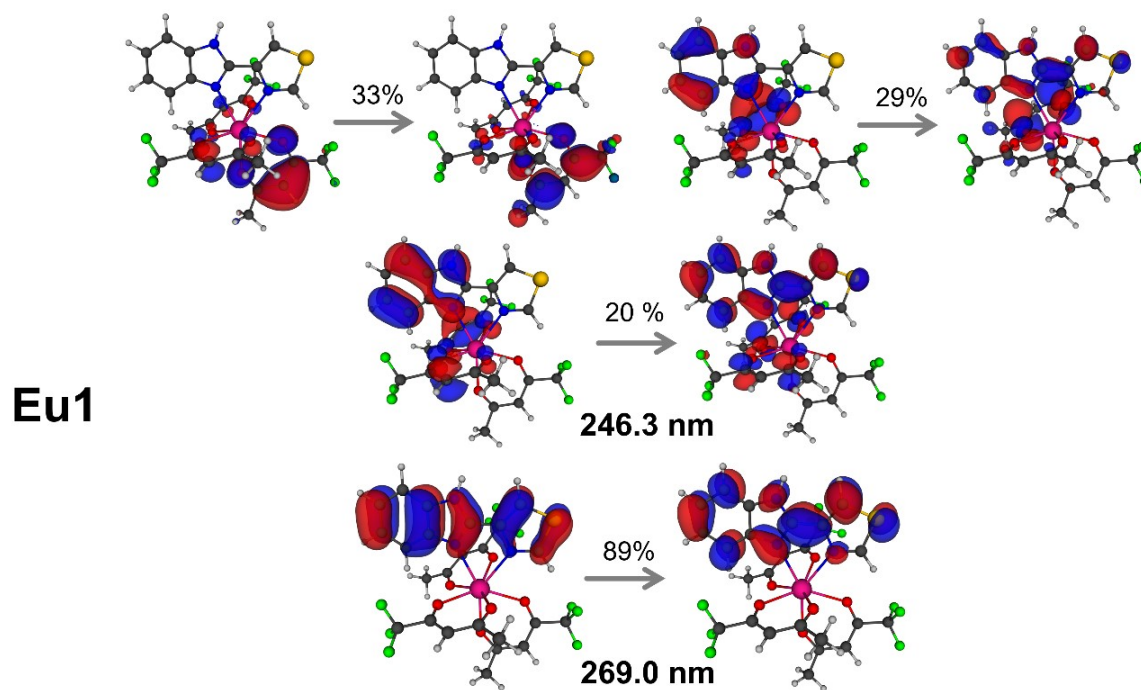
Fig. S6: Picture of the NTO mainly contributing to the most intense bands of **Eu1** and **Eu2** calculated with the TD-DFT CAM-B3LYP/TZVPPD/MWB52 (DCM) method. The percentages indicate the contribution of the main NTO for each transition.

Eu1

HOMO-4 HOMO-3 HOMO-2

HOMO-1 HOMO LUMO

LUMO+1 LUMO+2 LUMO+3

Eu2

HOMO-4 HOMO-3 HOMO-2

HOMO-1 HOMO LUMO

LUMO+1 LUMO+2 LUMO+3
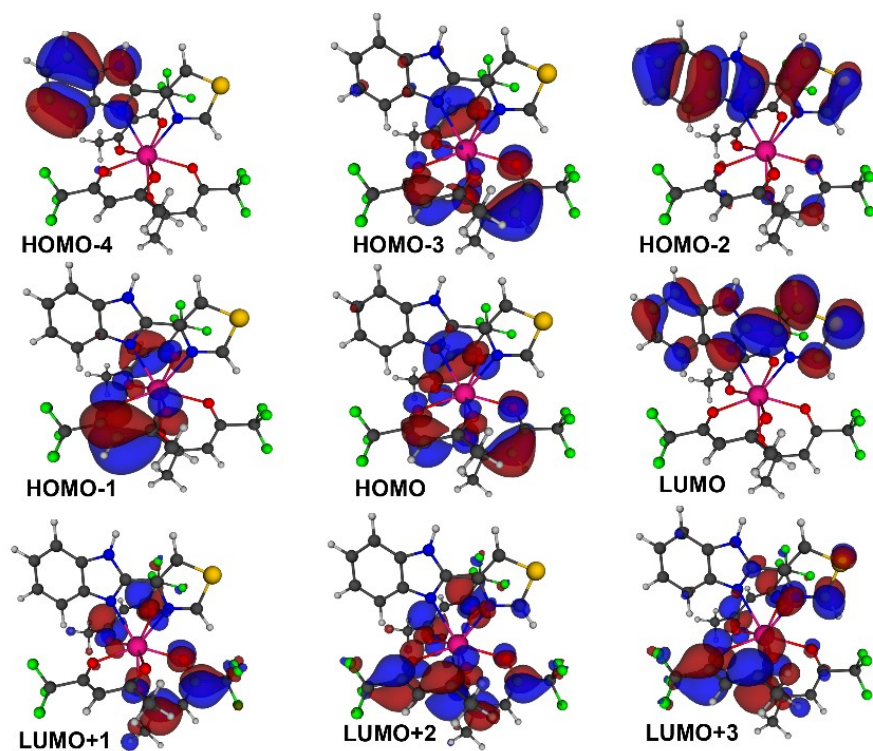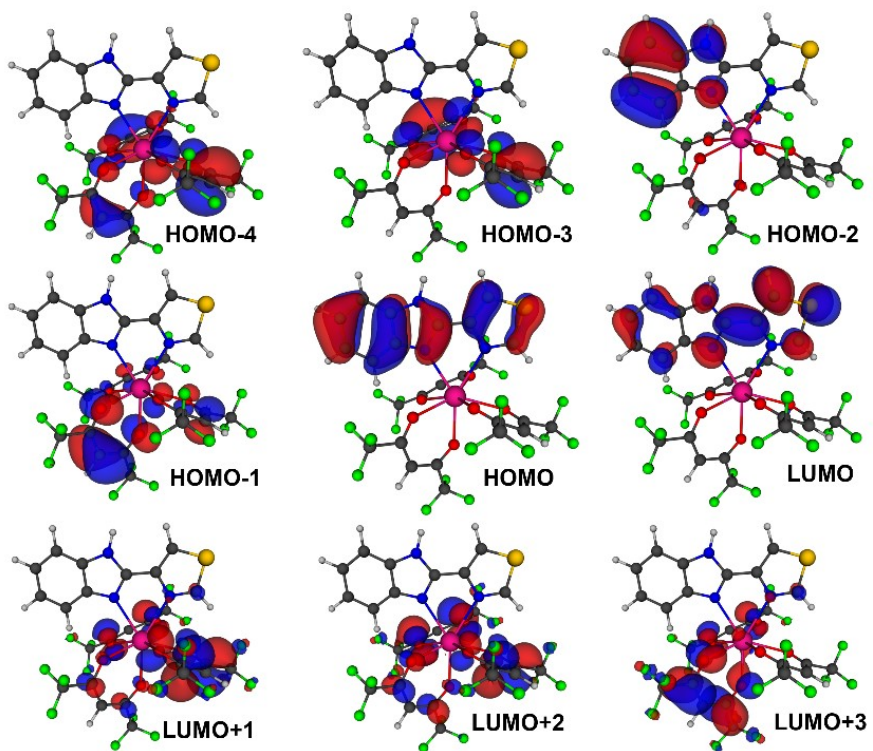
Fig. S7: Most relevant MOs calculated at the TD-DFT CAM-BLYP level of theory that explain the main electronic transitions, without considering the implicit effect of the DCM solvent.
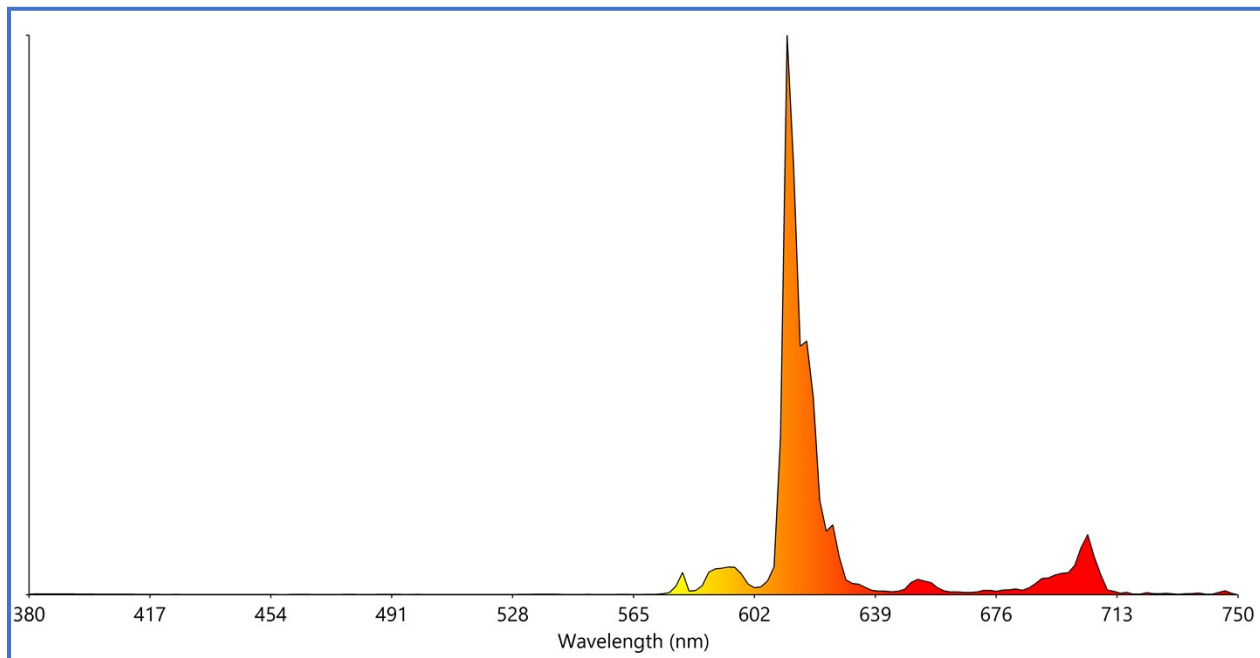
Fig. S8: Full PL spectrum of **Eu1** in DCM.
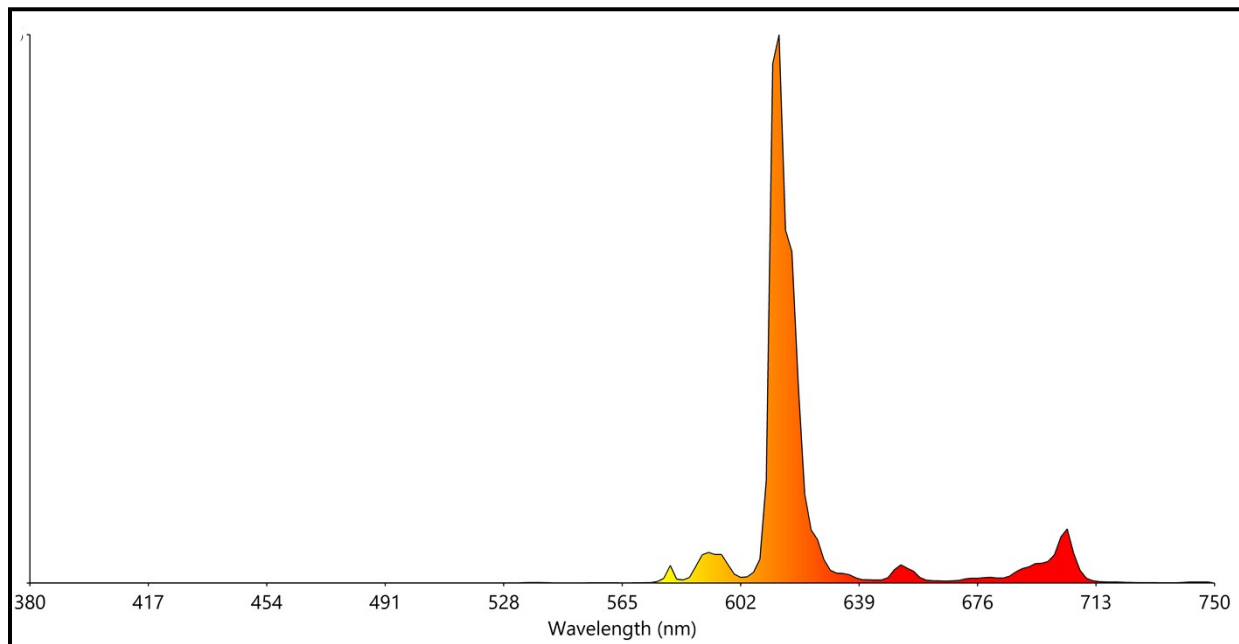
Fig. S9: Full PL spectrum of **Eu2** in DCM.
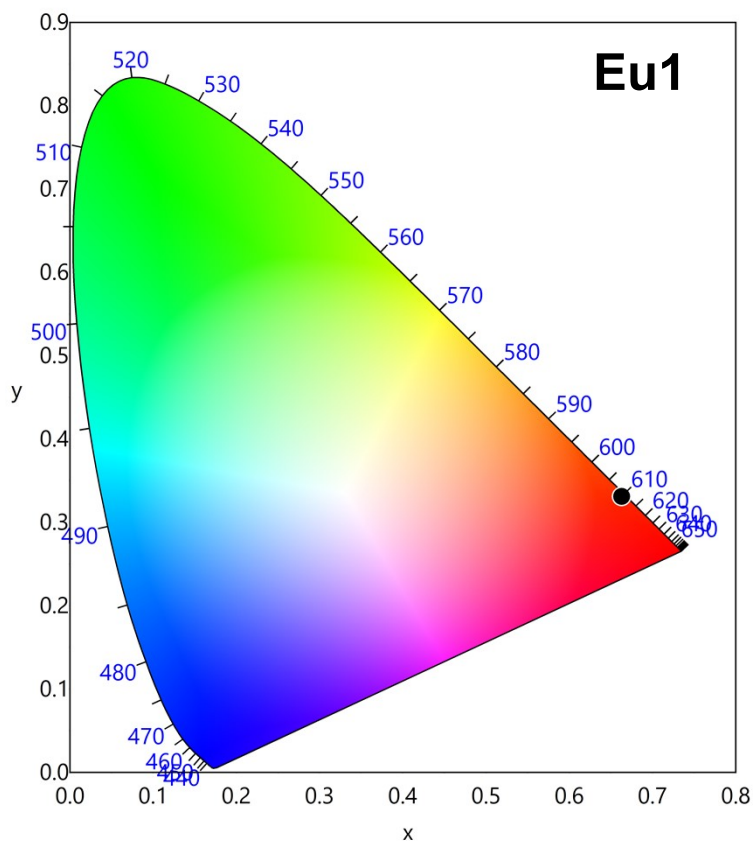
Fig. S10:   CIE-1931 chromaticity diagram demonstrating the calculated colour coordinate (x, y) values for **Eu1** in DCM at RT.
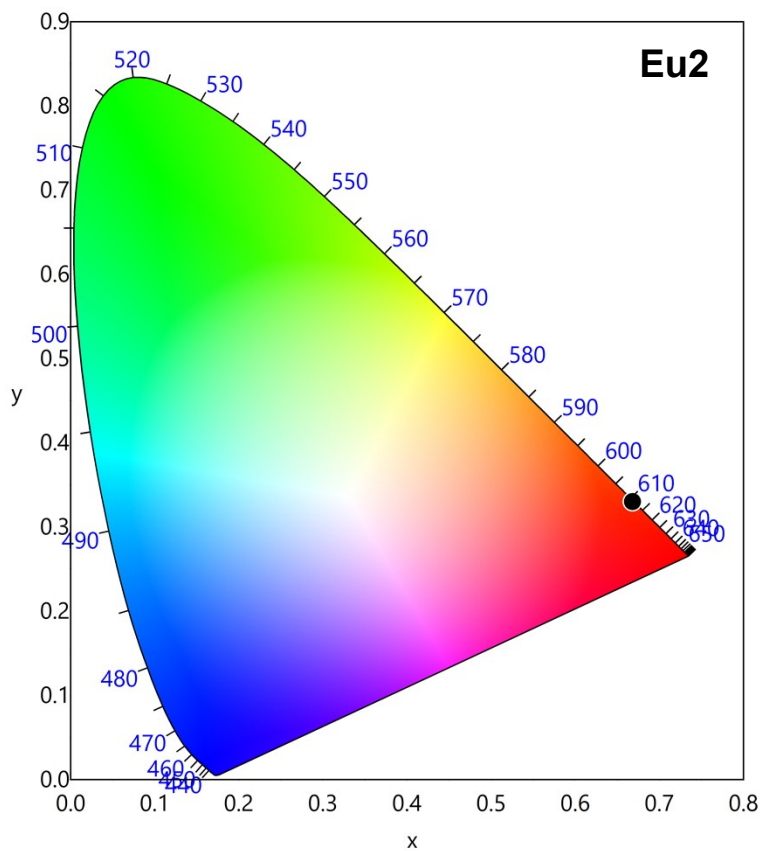
Fig. S11: CIE-1931 chromaticity diagram demonstrating the calculated colour coordinate (x, y) values for **Eu1** in DCM at RT.
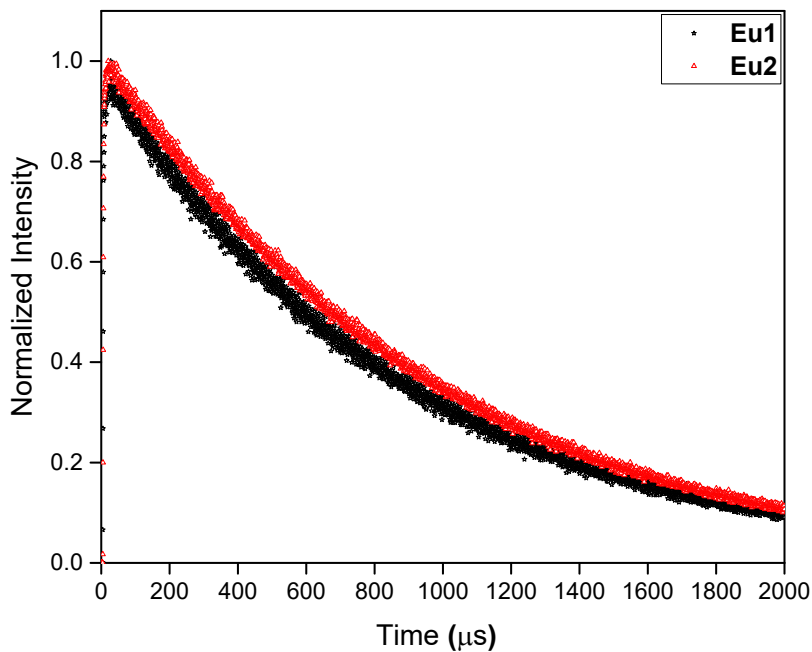
Fig. S12: Room temperature PL decay profiles of **Eu1** and **Eu2** in DCM.
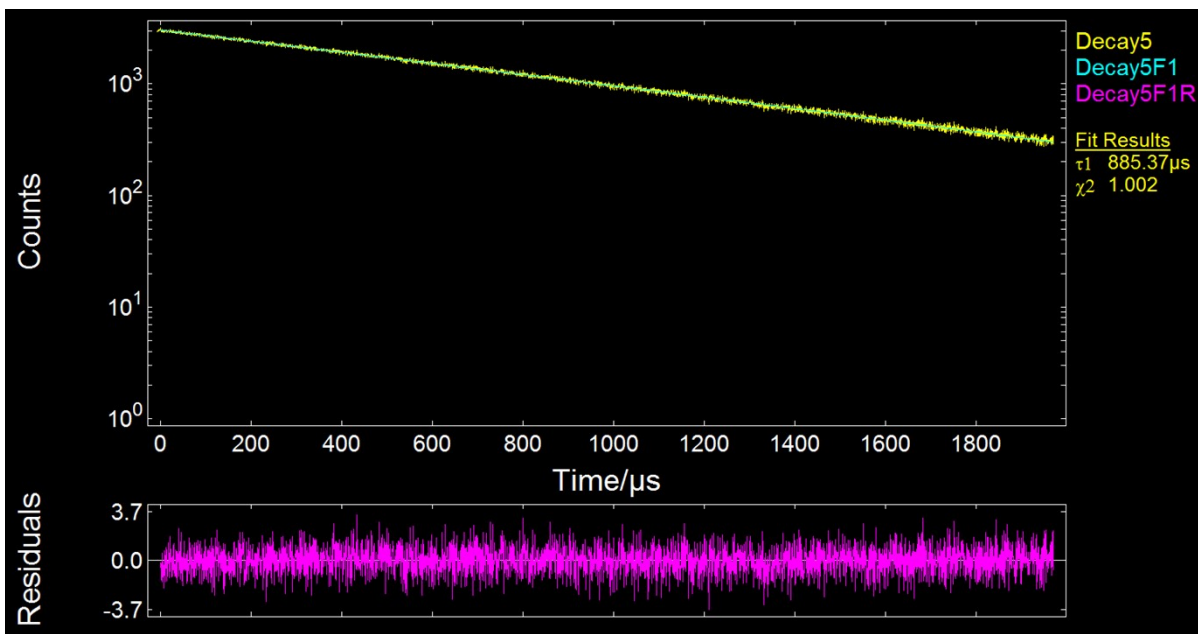
Fig. S13: Decay curve of **Eu1** with fitted curve and observed luminescence lifetime in DCM at room temperature.
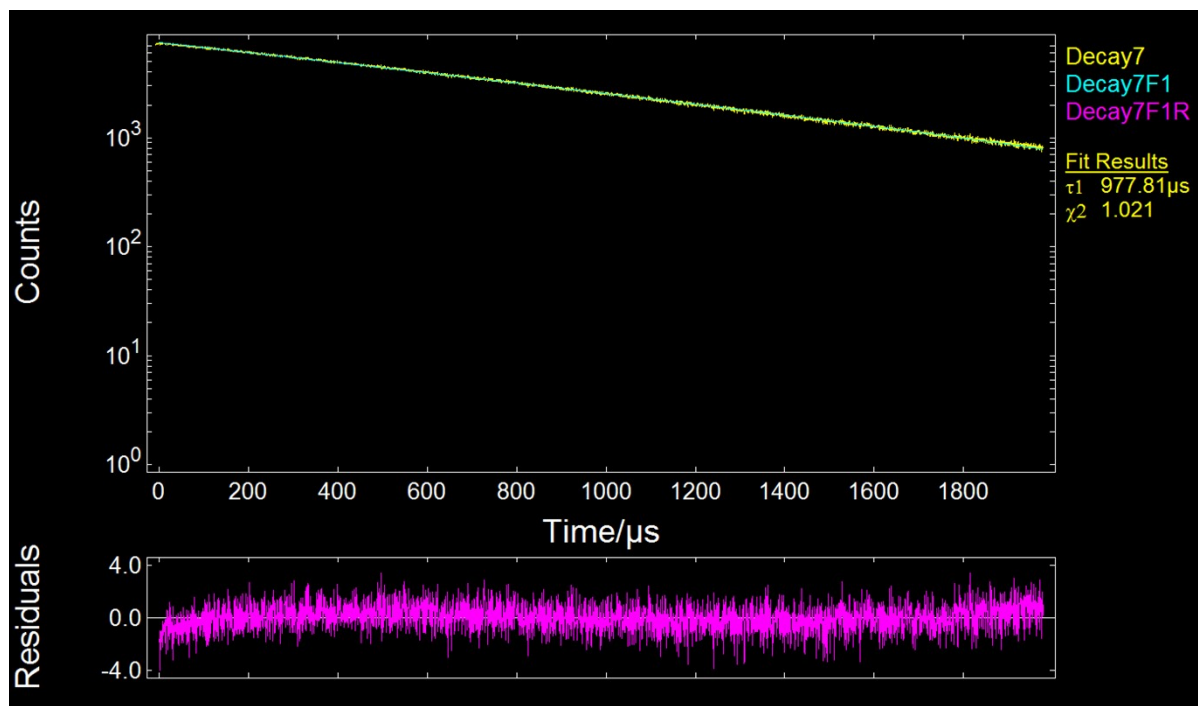
Fig. S14: Decay curve of **Eu2** with fitted curve and observed luminescence lifetime in DCM at room temperature.
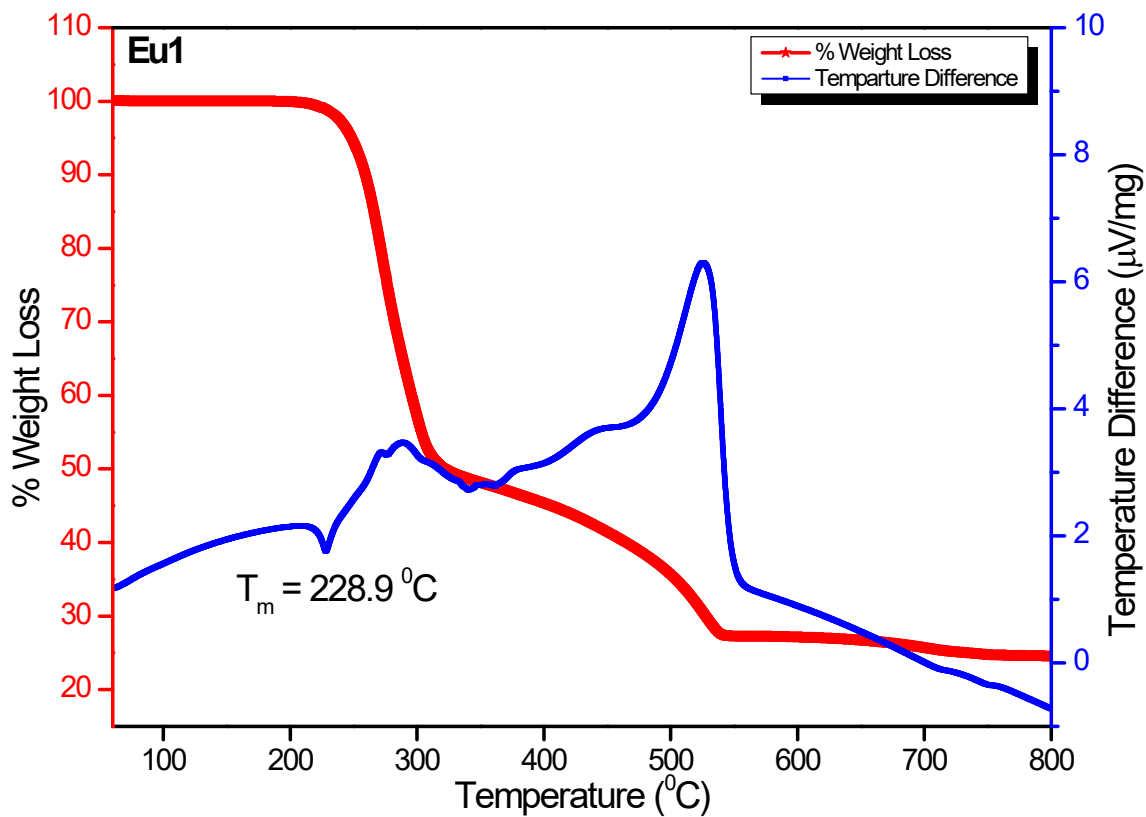
Fig.S15:   TGA and DTA profile of **Eu1** under N_2 atmosphere.

In the figure: $T_m = 228.9\ ^0C$
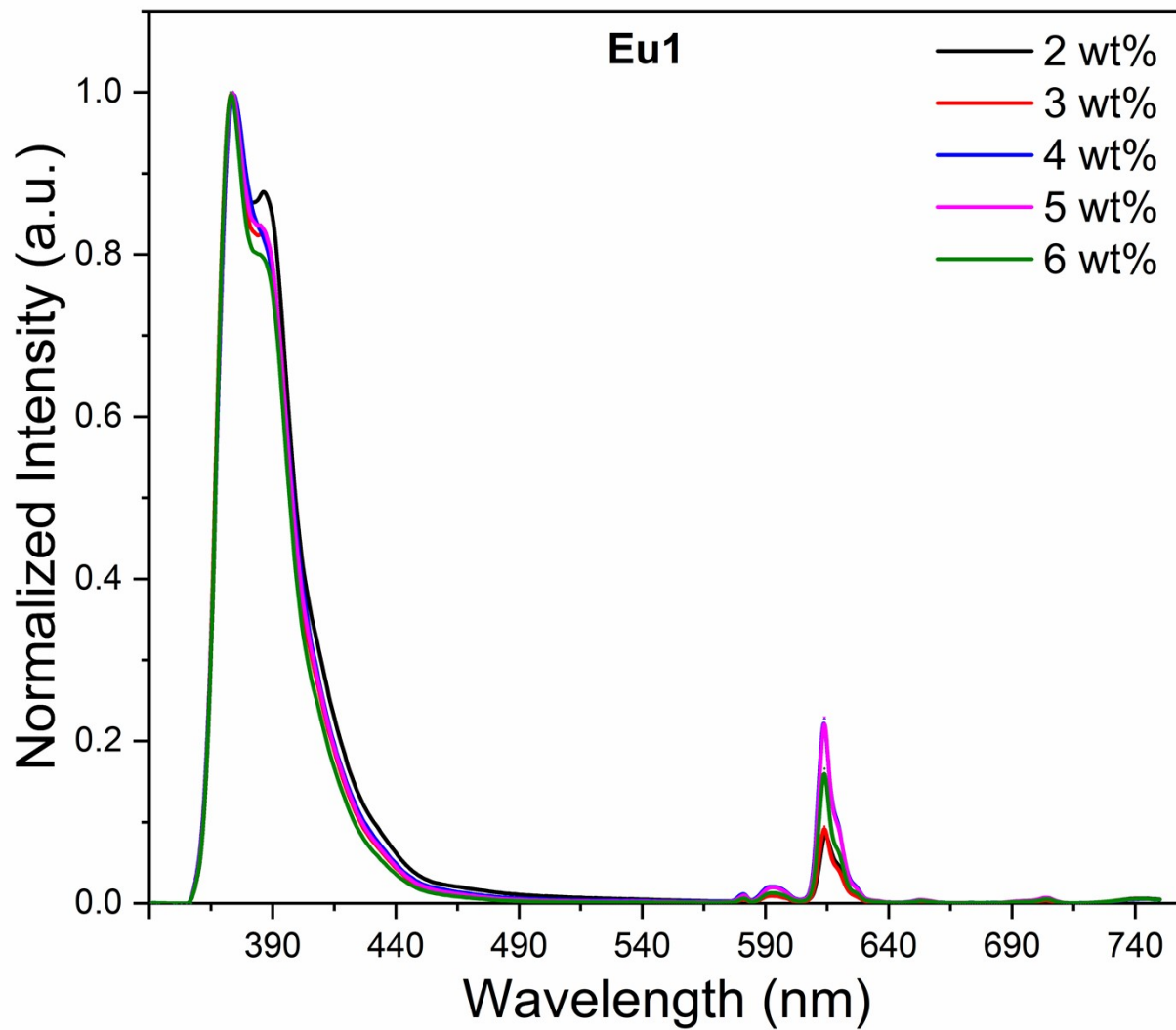
Fig. S16: PL spectra of the single EML doped film of **Eu1**.
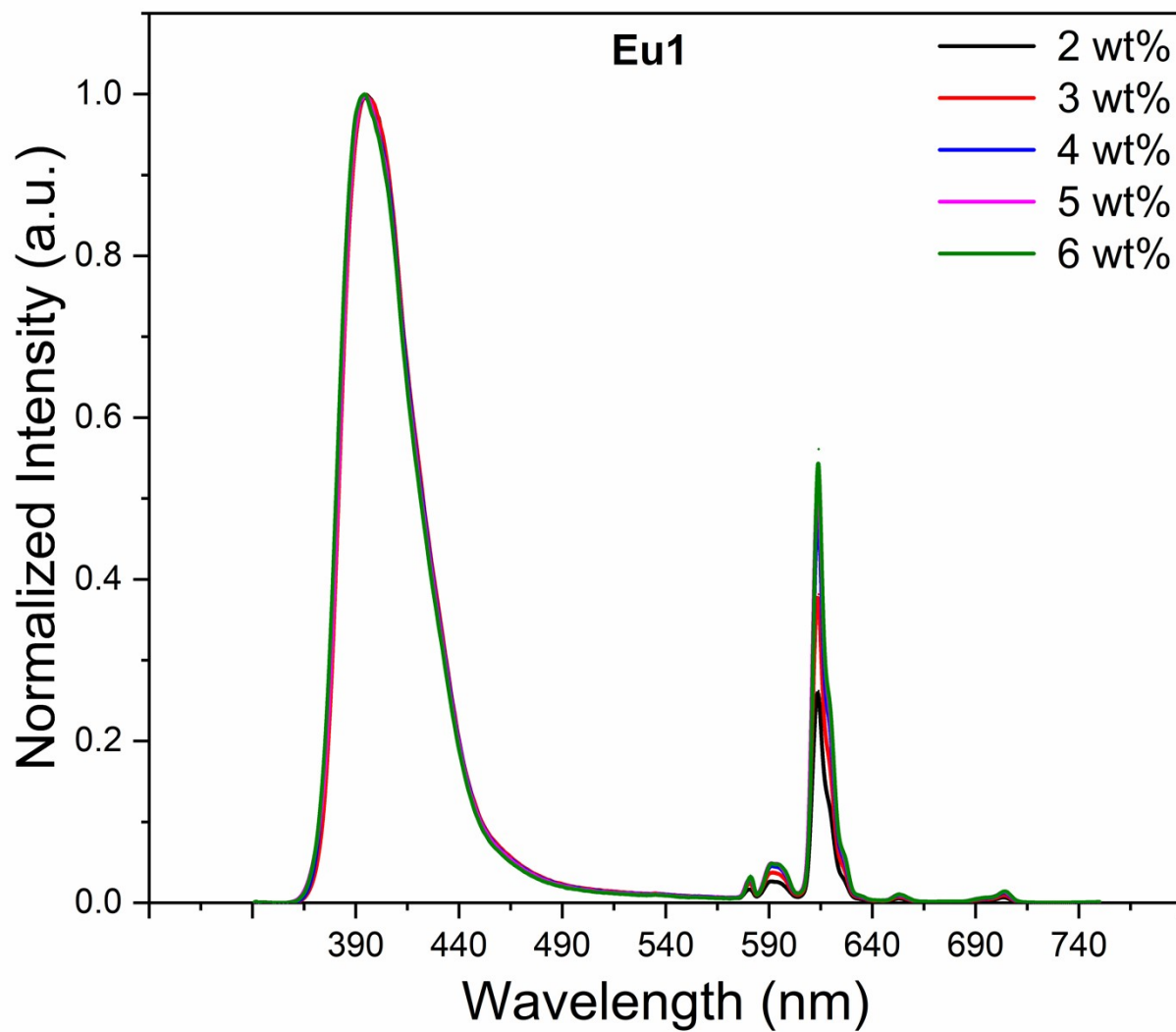
Fig. S17:   PL spectra of the double EML doped film of **Eu1**.
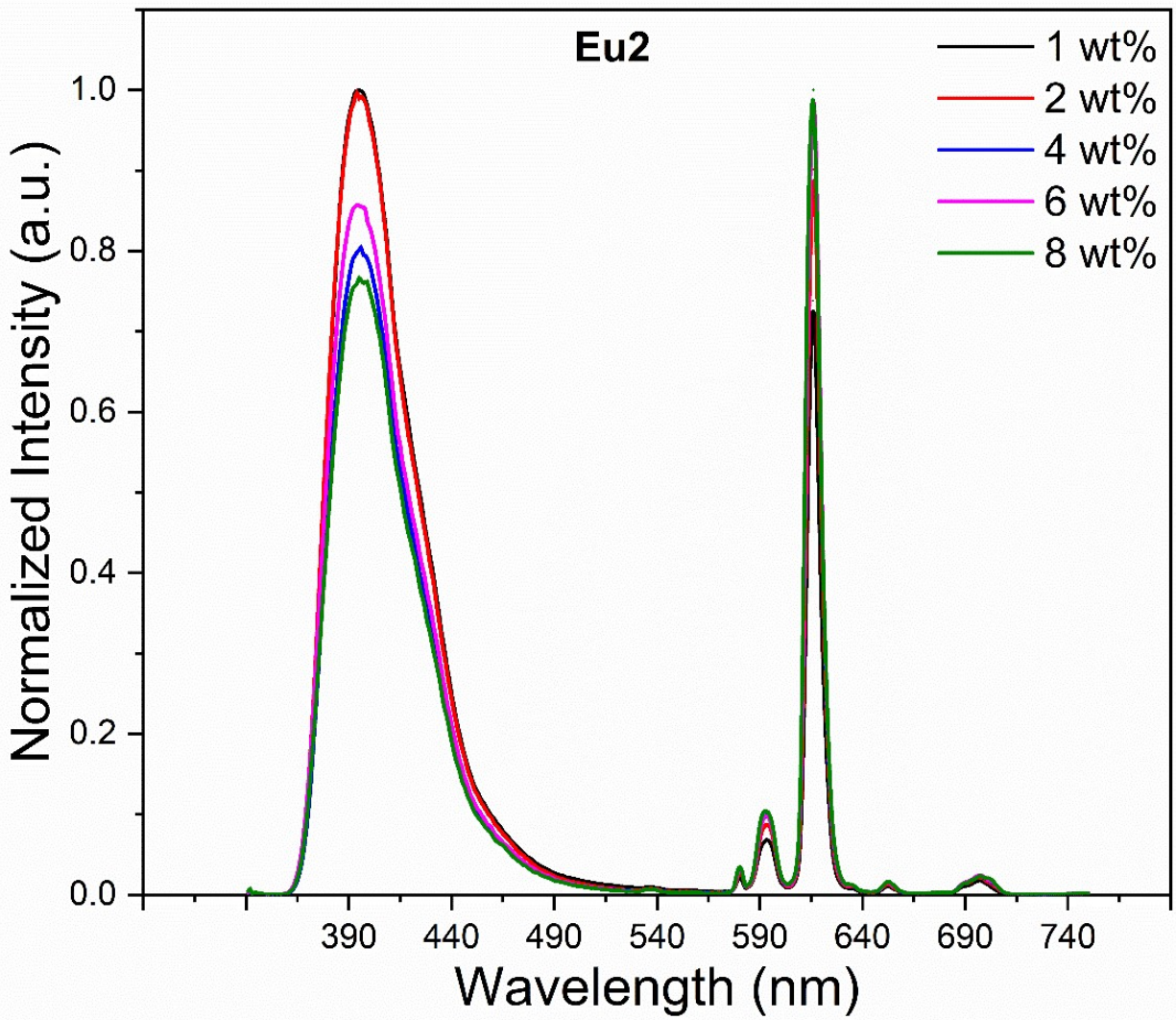
Fig. S18: PL spectra of the single EML doped film of **Eu2**.
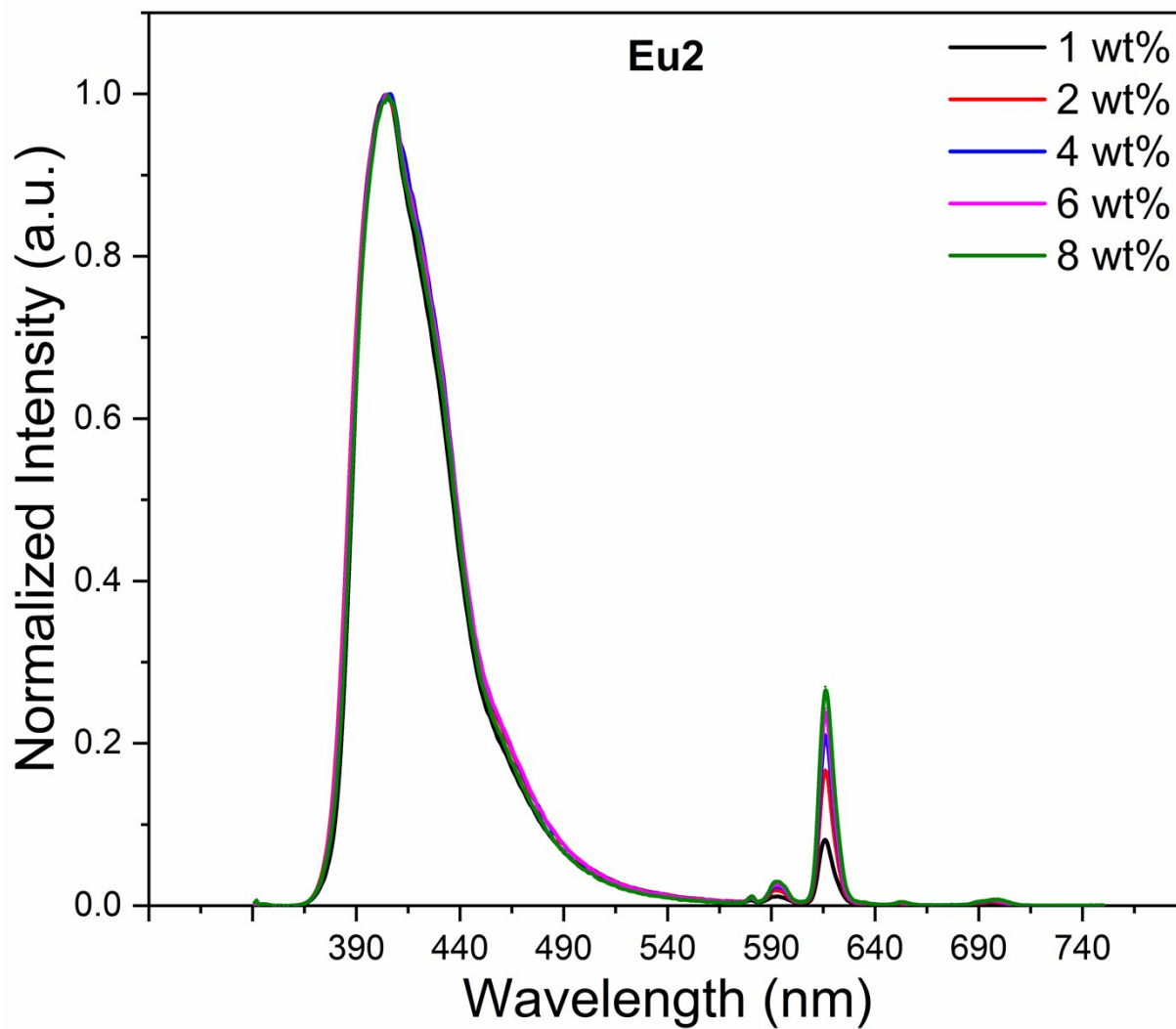
Fig. S19: PL spectra of the double EML doped film of **Eu2**.
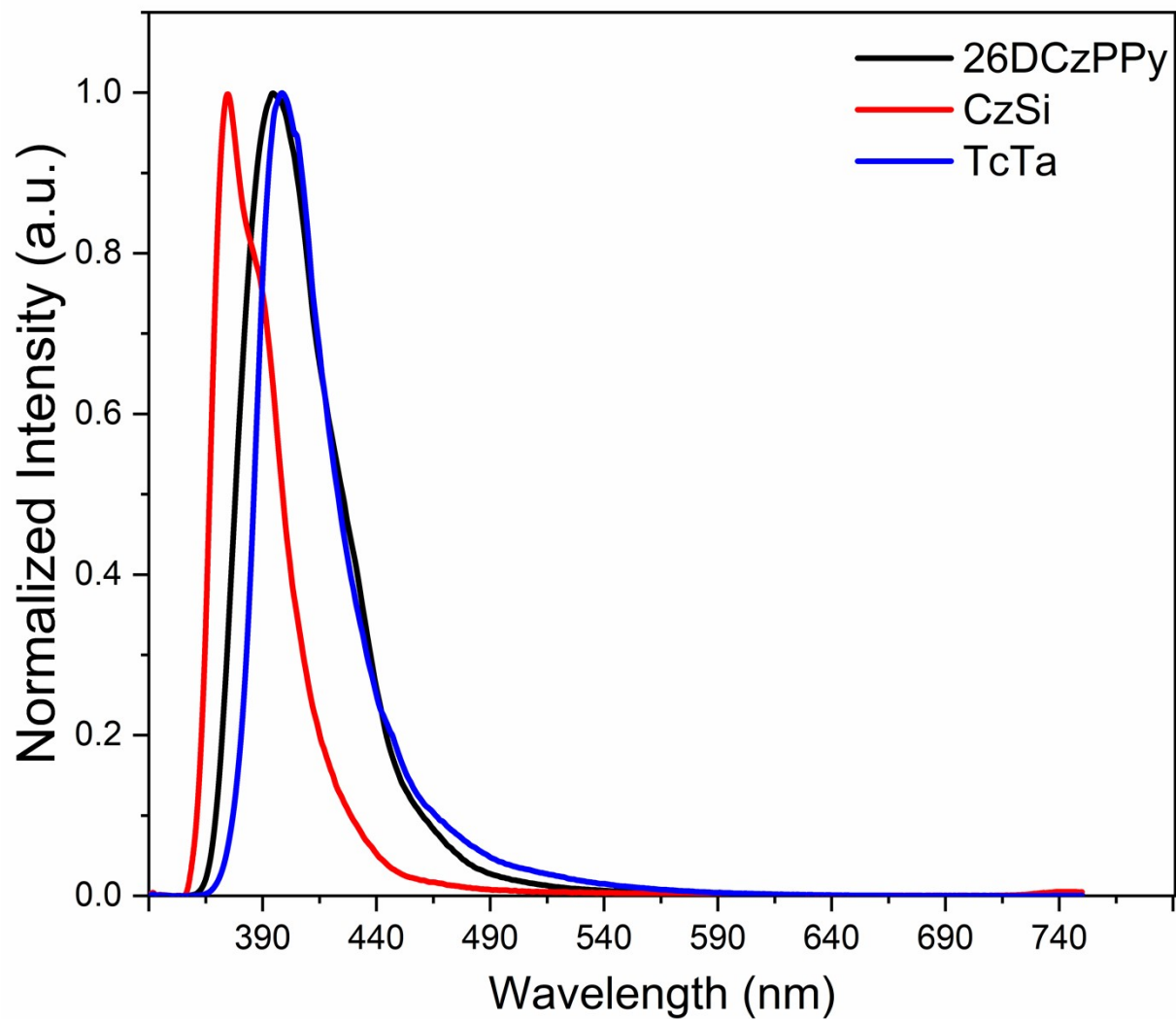
Fig. S20: PL spectra of host materials.
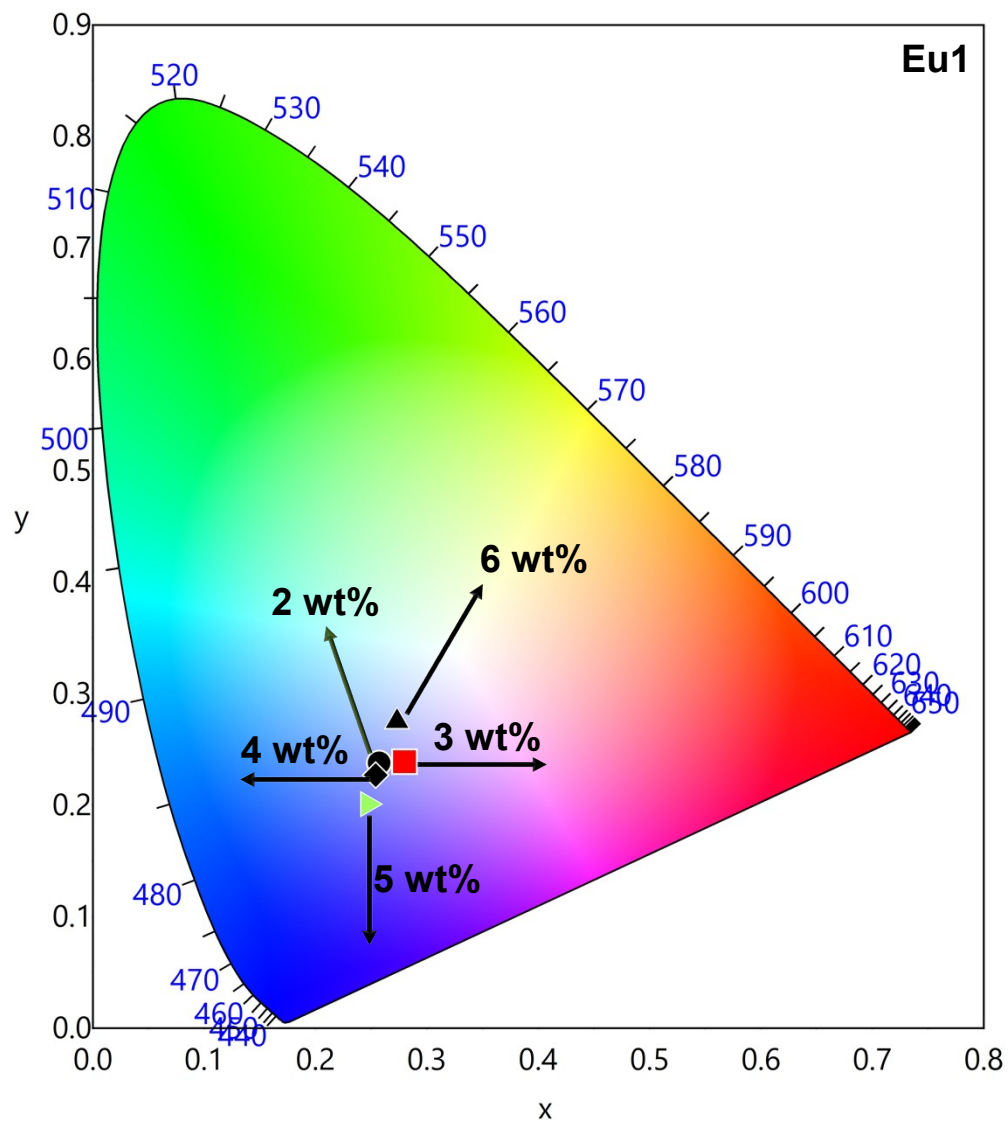
Fig. S21:   CIE 1931 chromaticity diagrams of double-EML **Eu1** based devices at different doping concentration operating at J = 10 mAcm^{-2}.
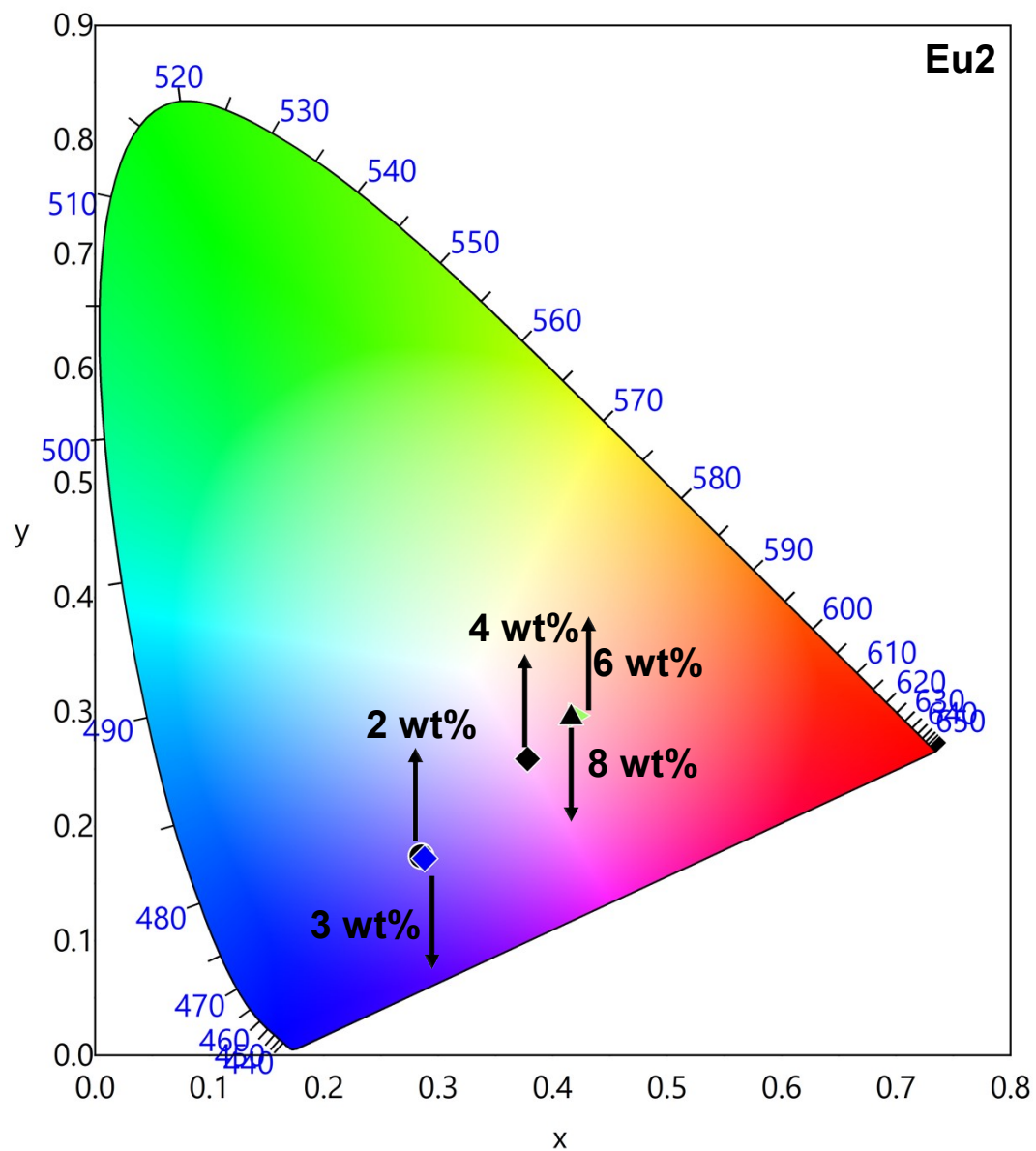
Fig. S22: CIE 1931 chromaticity diagrams of double-EML **Eu2** based devices at different doping concentration operating at J = 10 mAcm^{-2}.
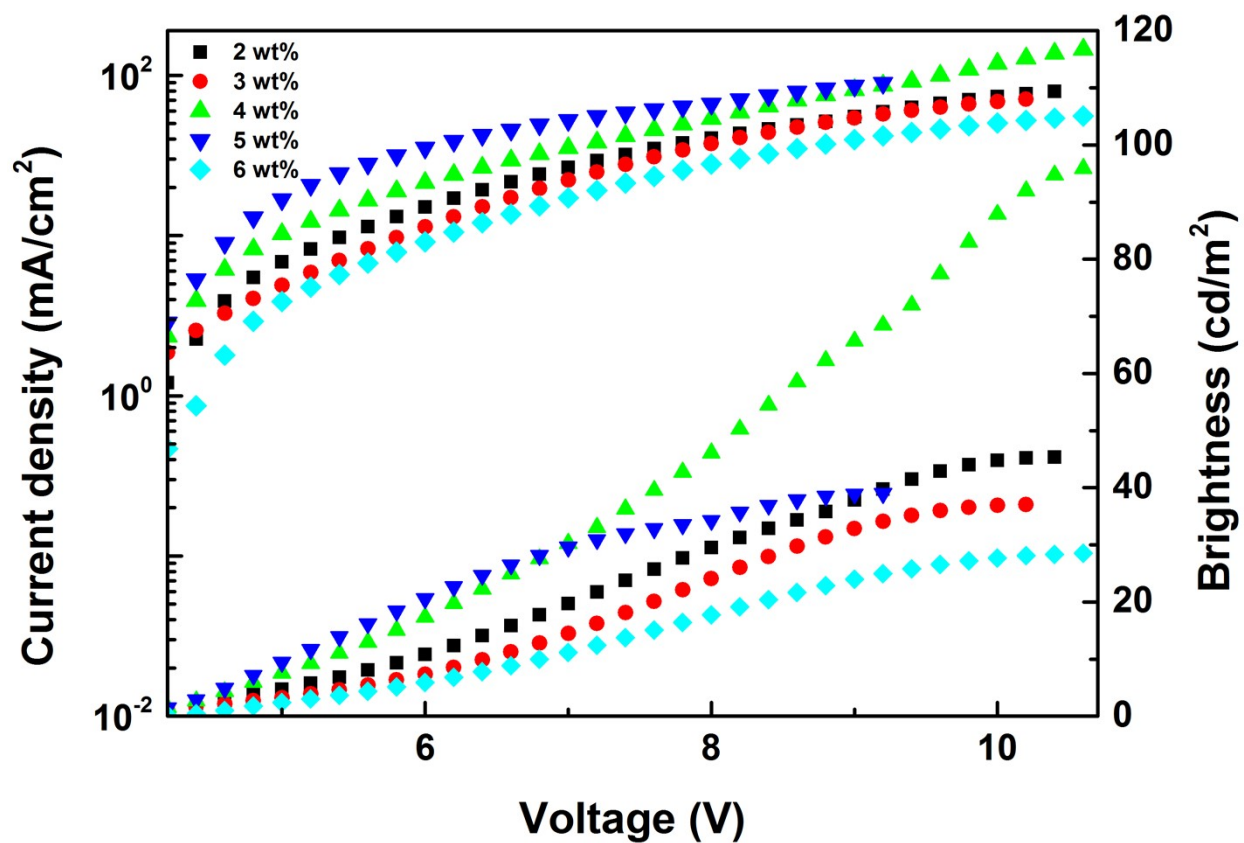
Fig. S23: Current density (J)-voltage (V)-brightness (B) curve of the double-EML OLEDs of **Eu1**.
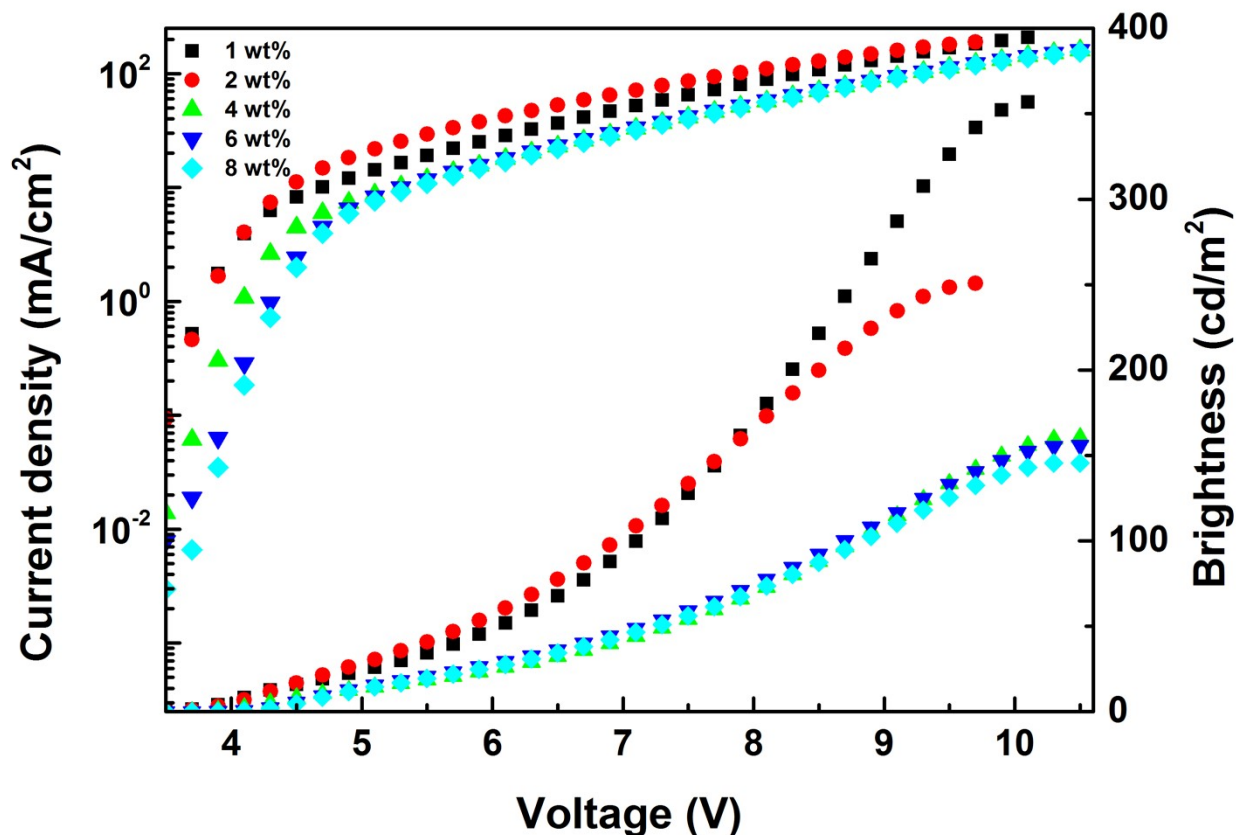
Fig. S24: Current density (J)-voltage (V)-brightness (B) curve of the double-EML OLEDs of **Eu2**.

References

1. F. Neese, *WIREs Computational Molecular Science*, 2022, **n/a**, e1606.

2. (a) R. Ilmi, W. Sun, J. D. L. Dutra, N. K. Al-Rasbi, L. Zhou, P.-C. Qian, W.-Y. Wong, P. R. Raithby and M. S. Khan, *J. Mater. Chem. C*, 2020, **8**, 9816-9827; (b) M. S. Khan, R. Ilmi, W. Sun, J. D. L. Dutra, W. F. Oliveira, L. Zhou, W.-Y. Wong and P. R. Raithby, *Journal of Materials Chemistry C*, 2020, **8**, 5600-5612; (c) I. J. Al-Busaidi, R. Ilmi, J. D. L. Dutra, W. F. Oliveira, A. Haque, N. K. Al Rasbi, F. Marken, P. R. Raithby and M. S. Khan, *Dalton Trans.*, 2021, **50**, 1465-1477; (d) I. J. Al-Busaidi, R. Ilmi, D. Zhang, J. D. L. Dutra, W. F. Oliveira, N. K. Al Rasbi, L. Zhou, W.-Y. Wong, P. R. Raithby and M. S. Khan, *Dyes Pigm.*, 2022, **197**, 109879; (e) A. S. Borges, J. D. L. Dutra, G. S. Santos, R. Diniz, J. Kai and M. H. Araujo, *Journal of Molecular Modeling*, 2021, **27**, 293.

3. M. Dolg, H. Stoll, A. Savin and H. Preuss, *Theoretica Chimica Acta*, 1989, **75**, 173-194.

4. (a) J. E. Ridley and M. C. Zerner, *Theoretica Chimica Acta*, 1976, **42**, 223-236; (b) A. V. M. de Andrade, R. L. Longo, A. M. Simas and G. F. de Sa, *Journal of the Chemical Society-Faraday Transactions*, 1996, **92**, 1835-1839.

5. J. D. L. Dutra, T. D. Bispo and R. O. Freire, *Journal of Computational Chemistry*, 2014, **35**, 772-775.

6. (a) O. L. Malta, *J. Lumin.*, 1997, **71**, 229-236; (b) F. R. G. E. Silva and O. L. Malta, *J. Alloys Compd.*, 1997, **250**, 427-430.

7. A. N. Carneiro Neto, E. E. S. Teotonio, G. F. de Sá, H. F. Brito, J. Legendziewicz, L. D. Carlos, M. C. F. C. Felinto, P. Gawryszewska, R. T. Moura, R. L. Longo, W. M. Faustino and O. L. Malta, in *Handbook on the Physics and Chemistry of Rare Earths*, eds. J.-C. G. Bünzli and V. K. Pecharsky, Elsevier, 2019, vol. 56, pp. 55-162.

8. A. J. Freeman and J. P. Desclaux, *Journal of Magnetism and Magnetic Materials*, 1979, **12**, 11-21.

9. O. L. Malta and F. R. G. E. Silva, *Spectrochimica Acta Part A-Molecular and Biomolecular Spectroscopy*, 1998, **54**, 1593-1599.

10. O. L. Malta, *Journal of Non-Crystalline Solids*, 2008, **354**, 4770-4776.

11. E. Kasprzycka, A. N. Carneiro Neto, V. A. Trush, L. Jerzykiewicz, V. M. Amirkhanov, O. L. Malta, J. Legendziewicz and P. Gawryszewska, *Journal of Rare Earths*, 2020, **38**, 552-563.

12. O. L. Malta, *Chemical Physics Letters*, 1982, **88**, 353-356.

13. O. L. Malta, S. J. L. Ribeiro, M. Faucher and P. Porcher, *Journal of Physics and Chemistry of Solids*, 1991, **52**, 587-593.

14. O. L. Malta, *Chem. Phys. Lett.*, 1982, **87**, 27-29.

15. J. D. L. Dutra, N. B. D. Lima, R. O. Freire and A. M. Simas, *Scientific Reports*, 2015, **5**, 13695.

16. M. A. Filho, J. D. L. Dutra, H. L. Cavalcanti, G. B. Rocha, A. M. Simas and R. O. Freire, *Journal of Chemical Theory and Computation*, 2014, **10**, 3031-3037.

17. J. J. P. Stewart, Stewart Computational Chemistry, Colorado Springs, CO, USA, 2016.

18. M. J. Weber, T. E. Varitimo and B. H. Matsinge, *Physical Review B*, 1973, **8**, 47-53.